Received: 12 December 2022 | Revised: 25 February 2023 | Accepted: 27 March 2023

DOI: 10.1002/elps.202200286

ELECTROPHORESIS

REVIEW

Electropatterning—Contemporary developments for selective particle arrangements employing electrokinetics

Adrian Lomeli-Martin[1] | **Nuzhet Ahamed**[1] | **Vinay V. Abhyankar**[2] | **Blanca H. Lapizco-Encinas**[1]

[1]Microscale Bioseparations Laboratory and Biomedical Engineering Department, Rochester Institute of Technology, Rochester, New York, USA

[2]Biological Microsystems Laboratory and Biomedical Engineering Department, Rochester Institute of Technology, Rochester, New York, USA

Correspondence
Vinay Abhyankar, Biological Microsystems Laboratory and Biomedical Engineering Department, Rochester Institute of Technology, 160 Lomb Memorial Drive, Rochester, NY 14623, USA.
Email: vvabme@rit.edu

Blanca H. Lapizco-Encinas, Microscale Bioseparations Laboratory and Biomedical Engineering Department, Rochester Institute of Technology, 160 Lomb Memorial Drive, Rochester, NY 14623, USA.
Email: bhlbme@rit.edu

Color online: See article online to view Figures 1–6 in color.

Funding information
NIH, Grant/Award Number: R21GM143658; NSF, Grant/Award Numbers: 2150798, 2127592

Abstract

The selective positioning and arrangement of distinct types of multiscale particles can be used in numerous applications in microfluidics, including integrated circuits, sensors and biochips. Electrokinetic (EK) techniques offer an extensive range of options for label-free manipulation and patterning of colloidal particles by exploiting the intrinsic electrical properties of the target of interest. EK-based techniques have been widely implemented in many recent studies, and various methodologies and microfluidic device designs have been developed to achieve patterning two- and three-dimensional (3D) patterned structures. This review provides an overview of the progress in electropatterning research during the last 5 years in the microfluidics arena. This article discusses the advances in the electropatterning of colloids, droplets, synthetic particles, cells, and gels. Each subsection analyzes the manipulation of the particles of interest via EK techniques such as electrophoresis and dielectrophoresis. The conclusions summarize recent advances and provide an outlook on the future of electropatterning in various fields of application, especially those with 3D arrangements as their end goal.

KEYWORDS
dielectrophoresis, electrokinetics, electropatterning, electrophoresis, microfluidics

Abbreviations: 2D, two dimensional; 3D, three dimensional; 3DEAL, 3D electrophoresis-assisted lithography; AC, alternating current; Alg, alginate; CEA, contraction/expansion; DC, direct current; DEP, dielectrophoresis; DI, deionized; EDL, electrical double layer; EF, electric field; EHD, electrohydrodynamic; EK, electrokinetic; eMAP, electro-microfluidic assembly platform; EO, electroosmosis; EP, electrophoresis; EPD, electrophoretic deposition; EPDD, electrophoretic control of discrete droplets; EWOD, electrowetting-on-dielectric; f, frequency of the electric field applied; f_{CM}, Clausius–Mossotti factor; FN, fibronectin; ITO, indium–titanium oxide; L-DEP, liquid dielectrophoresis; LDEPD, light-directed EPD; nDEP, negative-DEP; ODEP, optically induced DEP; PA–Colla, polyacrylamide–collagen; pDEP, positive-DEP; PEG, polyethylene glycol; rDEP, reservoir-based dielectrophoresis; SiN, silicon nitride; SMEs, spiral microelectrodes; UV, ultraviolet.

Adrian Lomeli-Martin and Nuzhet Ahamed contributed equally to this work.

1 | INTRODUCTION

Microfluidic devices have proven to be an excellent platform for assembling and manipulating microscopic objects, such as cells, colloids, droplets, proteins, and synthetic particles [1–4]. Microfluidic devices present general miniaturization benefits like fewer reagents, faster operation, parallel analysis, sensitive detection, and, relevant to this review article, the precise placement of objects down to the microscale (10^{-6}) [5, 6]. In the context of this review article, "patterning" refers to the generation of orderly arrangements within specified surfaces [7–9]. Patterning techniques are highly significant in many fields of science and technology with a wide range of applications. Some of these include the production of integrated circuits, microelectromechanical systems, miniaturized sensors, biochips, micro-optical components, and diffractive optical elements [10–13]. The design and patterning of structures close to the molecular level opens up the possibility for techniques with higher sensitivity applicable for the immobilization of biomolecules [14–17]. There is a growing demand for improvements in the complexity of the generated patterns; thus, significant efforts are being devoted toward the development of newer and innovative patterning techniques; each with their own set of benefits and shortcomings.

Patterning usually employs techniques like photolithography, laser, magnetic, electrokinetic (EK) manipulation, or a combination of several approaches [18–21]. Though these techniques are well-known and have been utilized to generate and replicate patterns, some have considerable limitations. Conventional photolithography processes are time-consuming, costly, and require sophisticated technologies to obtain accuracy and resolution in the microscale [22]. Laser-based methods have a limited focusing area and a need for high-power sources [23]. A significant limitation in magnetic field-based patterning lies in the requirement of pre-existing magnetic properties [24]. Although many techniques that use electric fields (EFs) rely on photolithographically patterned structures, they provide a series of unique advantages, such as robustness and simplicity, that make them attractive options for electropatterning [25]. Manipulating objects using EFs does not require any chemical modification or labels, making them compatible for the handling of biologically relevant materials [26–28]. EK manipulation also offers the ability to assemble particles into two-dimensional (2D) or even three-dimensional (3D) patterns in a variety of suspending solutions [29–32].

This review aims to compile and analyze recent (<5 years) advancements in patterning a wide array of particles by employing EK phenomena in microfluidic systems. In this article, patterning approaches that use EFs will be referred to as "electropatterning." The reports analyzed here include the deposition, orderly manipulation, and specific sorting of bioparticles. This review begins with simple colloidal arrangements and progresses to more complex macromolecular structures as EK properties may vary in size and structural complexity [33–36]. Although most of the compiled research studies have focused on manipulation by either electrophoresis (EP) or dielectrophoresis (DEP), some breakthroughs that combine these methods with other mechanical, optical, or magnetic forces are also included. Finally, the potential of EK manipulation techniques to achieve next-generation pattering capabilities is discussed.

2 | THEORY

In microfluidics, EK phenomena refer to the family of effects that occur when non-homogenous fluids are exposed to EFs [37]. These effects are attributed to the electrical double layer (EDL), which is the formation of two parallel layers of ions that surround a charged object exposed to electrolyte solutions [38]. The object could be, for example, a solid particle, a cell, a droplet, or similar. Although there are several ways in which EK phenomena may be categorized, for the purpose of this review these will be cataloged depending on the type of required EF distribution: (1) uniform and (2) nonuniform.

A system is under the influence of a uniform EF if the field strength is constant in the entire system [39]. The migration of particles under the effects of an EF is called EP [40], which requires particles to have an inherent electrical charge [41]. A basic EP-based system is formed by two electrodes of opposite charge, an anode (negative charge) and a cathode (positive charge), bridged by the presence of a conducting medium called an electrolyte solution. Besides the EP migration of particles, the presence of an EF also causes the "pumping" of liquid (electrolyte solution) inside the system by means of electroosmosis (EO); which is the result of the EK effects on the EDL of the capillary or microchannel wall [39]. Both EP and EO mobilities are a consequence of the zeta potential of the particle and the channel wall, respectively [42]. The EO motion of the fluid affects particles in the system and can even influence their aggregation [43]. The most basic configuration that employs these forces capillary electrophoresis system, which is shown in Figure 1A. The EDL, responsible for EO flow, is formed on the surface of the negatively charged capillary wall, and analytes and ions within the capillary migrate under the effects of both EP and EO. The resulting migration direction of the analytes depends on the relative magnitude of both phenomena [42]. The expressions of the

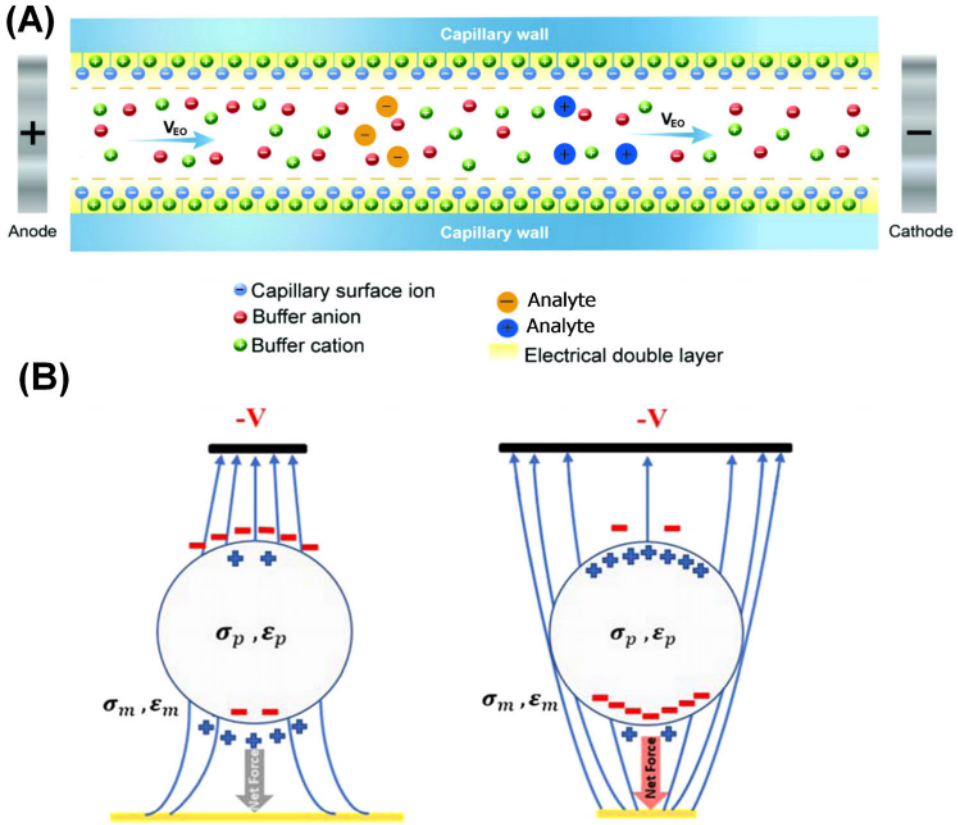

FIGURE 1 (A) Illustration of the electrokinetic (EK) forces present in a capillary electrophoresis (CE) system and a depiction of the electrical double layer (EDL) formed on the surface of the negatively charged capillary wall, the ions in the electrolyte and the analytes. (B) Illustration of the direction of the net dielectrophoresis (DEP) exerted on a particle exposed to a nonuniform electric field, negative DEP (left), and positive DEP (right). *Source*: Adapted with permission from Ref. [47], copyright (2020) Springer Nature.

linear EP and EP velocities are as follows:

$$\mathbf{v}_{EP} = \mu_{EP}\mathbf{E} = \frac{\varepsilon_m \zeta_P \mathbf{E}}{\eta} \quad (1)$$

$$\mathbf{v}_{EO} = \mu_{EO}\mathbf{E} = -\frac{\varepsilon_m \zeta_W \mathbf{E}}{\eta} \quad (2)$$

where μ represents mobility, ε_m is the electric permittivity of the medium, ζ is the particle or wall zeta potential, η is the medium viscosity and $\mathbf{E}$ is the EF. In systems where the EF distribution is nonuniform, which can be caused by the presence of insulating structures or specific electrode configurations, the EK phenomenon of DEP arises [44]. DEP is defined as the motion of particles as a result of polarization effects when the particle is exposed to a nonuniform EF; thus, DEP depends on the EF gradient ($\nabla \mathbf{E}^2$) [42]. As DEP does not depend on electrical charge, DEP is capable of manipulating neutral particles [45]. The expression of the DEP velocity ($\mathbf{v}_{DEP}$) for a spherical particle is shown in the following equation:

$$\mathbf{v}_{DEP} = \frac{r_p^2 \varepsilon_m}{3\eta} \mathrm{Re}\left[f_{CM}\right] \nabla \mathbf{E}^2 \quad (3)$$

where r_p is the particle radius, $\mathrm{Re}[f_{CM}]$ is the real part of the Clausius–Mossotti factor (f_{CM}), which accounts for the particle polarizability relative to the suspending medium. The expression for f_{CM} is described in the following equation [46]:

$$f_{CM} = \left[\frac{\varepsilon_p^* - \varepsilon_m^*}{\varepsilon_p^* + 2\varepsilon_m^*}\right] \quad (4)$$

where ε_p^* and ε_m^* are the complex permittivities ($\varepsilon^* = \varepsilon - (j\sigma/\omega)$) of the particle and medium, respectively; where ε and σ are, respectively, the permittivity and conductivity, $j = \sqrt{-1}$ and ω is the angular frequency of the EF. The direction of the DEP migration is dictated by the f_{CM}, which depends on the properties of the particle and media and the frequency of the EF [46]. Depending on its direction, DEP migration can be categorized as positive-DEP (pDEP) and negative-DEP (nDEP). In pDEP, particles migrate toward the regions with the highest field intensity, whereas in nDEP, particles migrate away from these regions, as shown in Figure 1B.

3 | COLLOIDS

Colloids are defined as mixtures in which microscopically dispersed insoluble particles of a substance (dispersed phase) are suspended in a dispersion medium (continuous phase). In colloidal suspensions, Brownian motion is the primary determinant of movement of the dispersed phase over time. Larger particles are more driven by buoyancy, whereas smaller ones by quantum effects [48]. The usual size range of the dispersed phase particles is between 1 nm and 1 μm in diameter [49]. However, in some instances, particles of size up to several tens of micrometers have also been reported as colloids [50]. The manipulation and assembly of colloids into higher order architectures has been an active research area due to the importance of colloidal particles in applications such as coatings, sensors, photonics, and electrical devices [51, 52]. The importance of these assemblies is attributed to their specific characteristics such as high packing density, high surface-to-volume ratio, potential for orientational interactions, and maximal structural stability [53–55]. Some of the most notable routes for assembling colloids include sedimentation, forced convection, template-assisted accumulation, Langmuir–Blodgett deposition, and the use of external electrical, magnetic, or optical fields [51, 56]. Due to their generality, higher throughput, and ease of implementation, EK-based techniques using EP and DEP phenomena offer attractive advantages over conventional methodologies [51, 57]. Recent studies that explored EP and DEP-based frameworks to create colloidal assemblies are discussed in the following subsections.

3.1 | Electrophoretic-based patterning of colloids

The formation of highly structured colloidal arrays using EP has garnered significant attention as a result of its high controllability, which is achieved by varying the size of the colloidal particles [58]. One of the most rapid and cost-effective EP-based techniques for creating dense and highly ordered colloidal assemblies is electrophoretic deposition (EPD) [59]. This technique refers to the controlled aggregation of particles moving under the influence of an EF [60]. In these systems, the aggregation rate depended on particle properties (zeta potential), experimental parameters (EF amplitude), and on the suspending media composition [61]. A recent study that employed EPD to obtain highly structured silver colloids was reported by Bi and Qi [59]. They used laser ablation on a silver plate that was submerged in pure water and observed the formation of well-defined sub-microscale silver peroxide (Ag_2O_2) cuboids on the anode surface. The Ag_2O_2 cuboid formation mechanism was attributed to two critical steps. First, the movement of the charged Ag ions to the cathode surface provoked an electrochemical oxidation reaction of Ag_2O_2 nanoparticles to occur. Second, the fusion of neighboring Ag_2O_2 nanoparticles created sub-microscale Ag_2O_2 particles through oxidization and oriented attachment. An image of the cuboids of Ag_2O_2 deposited on the electrode surface is shown in Figure 2A, which was obtained at a current density of 100 $\mu A/cm^2$. This study proposed a new growth mechanism using EPD that allowed for a constant deposition of metal oxide nanoparticles. However, this deposition was only achievable for 2D structures [59]. This limitation was addressed in a study by Muto et al. [58] where EPD was used for the formation of 2D and 3D metallic oxide films. Composite particles of SiO_2–SiO_2 with two distinct particle sizes of 200 nm and 16 μm were electrostatically assembled by employing a simple EP cell chamber where two conductive pieces of tape were attached to a glass slide as electrodes. The suspension of SiO_2 particles was introduced in the chamber, and by combining alternating current (AC) and direct current (DC) EFs, particle oscillations were induced. The use of AC fields proved to be essential as employing only a DC EF resulted in the formation of a disordered structure with voids. By fine-tuning the amplitude and frequency of the applied AC potential, the 3D hexagonal close-packed structure seen in Figure 2B was obtained at a potential of 30 V amplitude at 1 Hz. This is the first published work that reports the formation of 2D and 3D closely packed arrays of SiO_2 using DC and AC EFs. These studies illustrate that well-ordered colloidal arrays can be obtained by means of EK phenomena.

Another patterning study that used AC EFs to induce EP was reported by Fernández-Mateo et al. [57]. They observed that AC EFs had a predominant effect on the wall repulsion of charged colloidal particles in microfluidic channels. This work aimed to understand the effect of varying the frequency of the applied field in the 50 Hz to 10 kHz range on the repulsion of carboxylate particles. Figure 2C shows the superimposed images of 3 μm carboxylate particles at four distinct frequencies at 80 kV/m and a control image. As observed, the extent of the particle depletion region is a strong function of EF frequency, and the most significant wall repulsion was exhibited at lower frequencies. It was demonstrated that DEP, the mechanism believed to be responsible for this repulsion, was only valid at high frequencies. Their results provided a conceptual understanding that hydrodynamic wall repulsion is the major contributing force to wall repulsion of charged colloidal particles during EP induced by AC EFs. This work represented a new potential strategy for the design of microfluidic technologies that use EFs for particle manipulation and separation.

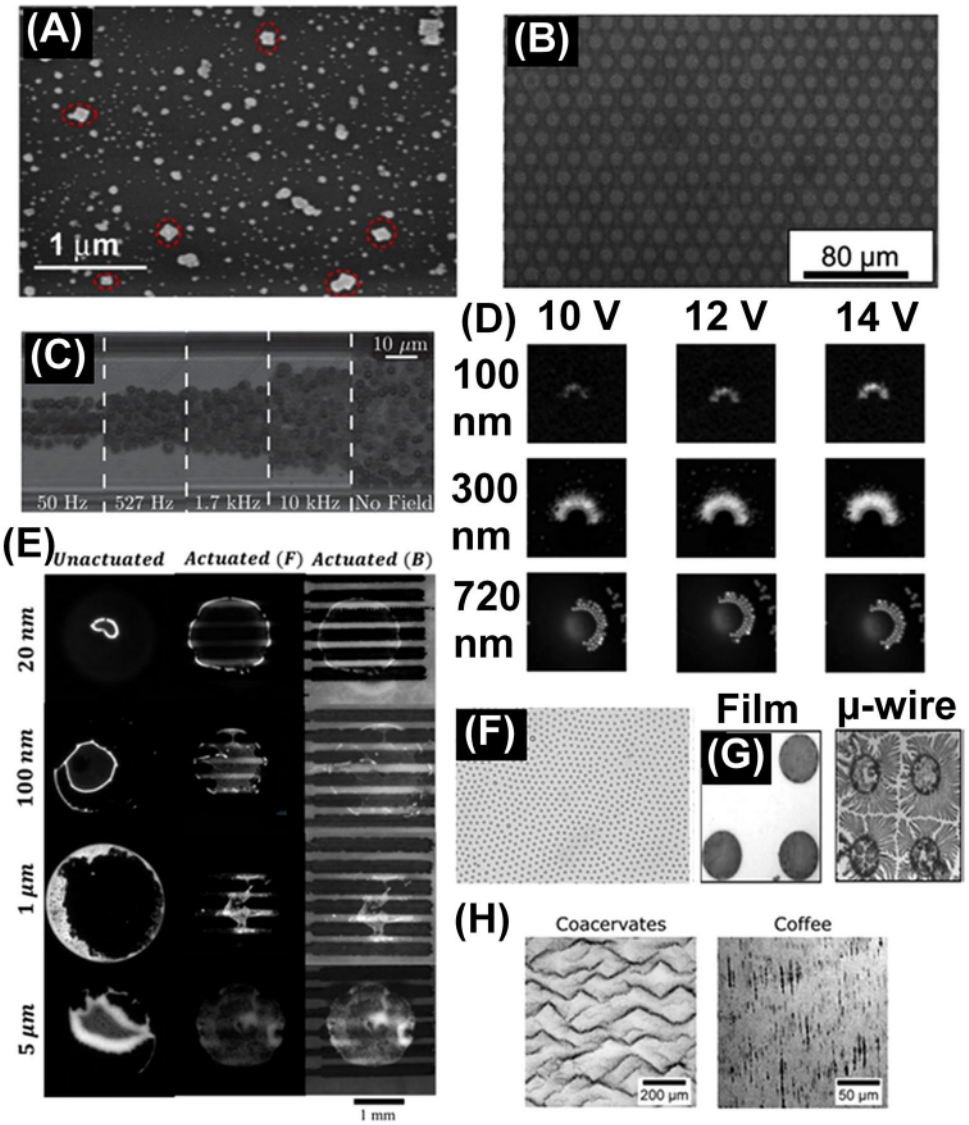

FIGURE 2 (A) Deposits of Ag_2O_2 formed on the electrode surface at 100 μA/cm^2. Dotted circles marked the quasi-cuboids. (B) Optical microscope images of electrostatically assembled SiO_2–SiO_2 composite films patterned with superimposition of alternating current (AC) and direct current (DC) electric fields (EFs). (C) Superimposed images illustrating the effects of wall repulsion on 3 μm carboxylate particles employing at four distinct frequencies; the fifth image was used as control. The particles were suspended in 1.7 mS/m KCl solution. (D) Microscope images of 100, 300, and 720 nm targets accumulated around a 15 μm Janus sphere for applied fields ranging between 10 and 14 V. (E) The demonstration of wing-like colloidal assembly polystyrene particles in water droplets, with increasing EF, *U* at a fixed frequency, frequency of the electric field applied (*f*) = 300 kHz. The upper row indicates the three-dimensional (3D) schematics of the putative assembly position, and the lower row shows the actual images of the 8 wt% polystyrene particles in a droplet of 274 μm diameter. (F) Two-dimensional (2D) non-closed-packed colloidal array of 700 nm polystyrene particles achieved with a 10 V_{pp} AC field at 1 kHz; scale bar: 20 μm. (G) Images of size- and frequency-dependent deposition of film and microwire obtained by the combined us of AC-dielectrophoresis (DEP) and AC-electrohydrodynamic (EHD) techniques at applied EF of 20 V_{pp}, 100 Hz for 5 min. (H) Images of band formation and zigzag patterns obtained in suspensions of coacervates and coffee colloids, by employing an AC EF of 17 mV/μm at 500 Hz and time of acquiring the images, $t = 100$ s. *Source*: (A) Adapted with permission from Ref. [59], copyright (2022) Elsevier. (B) Adapted with permission from Ref. [58], copyright (2022) Springer Nature. (C) Adapted with permission from Ref. [57], copyright (2022) American Physical society (APS). (D) Adapted from Ref. [62], open access article distributed under the Creative Commons Attribution (CC BY) License (2018). (E) Adapted from Ref. [63], open access article distributed under the Creative Commons Attribution (CC BY) License (2022). (F) Adapted with permission from Ref. [64], copyright (2017) American Chemical Society (ACS). (G) Adapted with permission from Ref. [51], copyright (2019) American Chemical Society (ACS). (H) Adapted with permission from [65], copyright (2022) American Physical Society (APS).

3.2 | Dielectrophoretic-based patterning of colloids

Colloids have numerous drug delivery applications as customized carriers for loading and transporting specific targets using DEP phenomena [62, 66]. The frequency tunability in DEP phenomena enables the unique flexibility to vary the choice of target *in situ*. A notable advancement in active colloid target selection was reported by Boymelgreen et al., where dynamic particle control was achieved with pDEP/nDEP [62]. They unified the tasks of loading and transporting multiple nano- and micro-sized targets. The first advantage of their approach was combining the loading and transport capabilities as a unified singular task instead of loading a target by one mechanism and then driving the transport with another mechanism. The second advantage was enabling the on-demand selection of multiple micro- and nano-sized targets without the need for pre-labeling or surface functionalization. Demonstrations of target accumulation and repulsion under the effect of pDEP and nDEP, respectively, can be seen in Figure 2D when applied EFs range from 10 to 14 V. By fine-tuning the frequency of the applied EF, the configuration of the colloidal particles can be selectively loaded/unloaded and dynamically modulated. This study illustrated the potential of combining dynamic selectivity with direct motion to develop fabrication techniques such as additive manufacturing and soft robotics.

Target selection is not the only application DEP has in the field of colloid manipulation. The assembly, transport, and deposition of colloidal particles can also be achieved by employing DEP, as can be seen in the work done by Shen et al. [63]. They reported an electro-microfluidic assembly platform (eMAP) for constructing and manipulating colloidal assemblies within water droplets. The main phenomena in their study for patterning these water-in-oil emulsions were DEP-induced droplet positioning, dielectrowetting-induced droplet deformation, and DEP colloidal assembly. They observed that upon application of AC voltage ranging from 0 to 130 V_{pp}, DEP and dielectrowetting phenomena started to act on the droplets. The authors state that, under these experimental conditions, there is a strong nDEP force acting upon the particle chains, resulting in a slight alteration to the chain orientation. Though there is a slight effect of the chain–chain interactions resulting from this change in orientation, the previously described wing-like structures are mainly governed by DEP in this assembly. This resulted in particle motion that enabled DEP-based colloidal assembly. These phenomena were used to manipulate motion and active colloid assembly. Various superstructures within water droplets were observed, which were further optimized by fine-tuning the inner fluidic and EFs along with the colloid properties. Figure 2E illustrates a "spreading wing" like 3D structure, where clusters of the polystyrene particle chains in the water droplets showed a wing-like pattern. This wing-like formation occurred as a response to increasing EF at a fixed frequency of 300 Hz as the direction of the DEP force exerted on particles can be adjusted by modifying the frequency of the applied EF. Overall, four distinct 3D colloidal assemblies were illustrated—the bottom base, wing-like, rising-chain-like, and top-cap-like structures. This controllable strategy was further extended to demonstrate the formation of anisotropic micro-gels from binary colloidal assembly and electrically driven optofluidic display devices.

3.3 | Hybrid systems employed for the patterning of colloids

Although EK techniques such as EP and DEP are able to form densely packed layers of colloidal particles, there is little control in the particle packing order within these layers, highlighting a major area of improvement [67–72]. The combination of multiple EK techniques within the same system has allowed higher control, resulting in the patterning of colloidal particles into advanced structures [51, 58, 64]. An investigation of the robustness of a coating process was done by Gong and Wu, where both AC and DC EFs were used for the manipulation of the colloidal arrays [64]. Their study showed that the application of low-frequency AC EFs induced dipolar repulsion among particles and resulted in an ordered, non-closed-packed colloidal array. Application of a simultaneous sequence of DC pulses combined with the low-frequency AC field–induced EP motion of the particles toward the substrate. An image of a 2D non-closed-packed colloidal arrays of 700 nm particles obtained with an AC EF of 10 V_{pp} at 1 kHz is shown in Figure 2F. This method is versatile, as it can also be used to create colloidal arrays with smaller particles, as long as the EF strength is strong enough to generate sufficient dipolar repulsion to overcome Brownian motion. The application of a sequence of DC pulses is also a commonly used technique to avoid solvent evaporation problems. This technique has the potential to be adopted in applications requiring a continuous convective method for scalable production of non-closed-packed 2D particle arrays.

As previously stated in Section 3.1, AC EFs have the added advantage of high-frequency tunability of particle pattern formation when compared to DC. This was further proved by the work of Goel et al., where the authors combined AC-dielectrophoresis (DEP) alongside AC-electrohydrodynamic (EHD) effects in a microwell for the manipulation of gold nanoparticles [51]. This work

demonstrated, in addition to the dependence that AC-DEP and AC-EHD forces have on the amplitude of the EF, the first scales with both particle size and field frequency, whereas the latter depends only on the field frequency. The results indicated that the colloidal structures transition from films to microwires as the particle diameters increase from nanometers to micrometers, with no observable assembly at intermediate particle sizes. The main finding of this work was the identification of the processes that governed the film and microwire formations. Film formation was purely governed by EHD forces occurring at the material's surface depositing submicron particles, whereas the microwire synthesis was a product of EHD-assisted-DEP forces present in larger particles. The two images in Figure 2G illustrate the size and frequency-dependent phase chart for film to microwire transition when an AC EF of 20 V_{pp} was applied, with maximum assembly obtained in the frequency range of 100–500 Hz. This study illustrated a simple and robust method for creating biosensing platforms with applications in chemical studies, nanoelectronics, and pathogen capture and analysis. Another study in which AC EFs were used for the formation of patterns in colloids was reported by Katzmeier et al. [65]. Here, a combination of EK flow and hydrodynamic interactions resulted in the formation of patterns in a wide range of colloidal particles. Figure 2H contains two example images illustrating both band formations and a zigzag pattern of coacervates and coffee colloids obtained by employing an AC EF of 17 mV/μm at a frequency of 500 Hz, and the image acquisition time being 100 s. This study provided a better understanding of the physical mechanisms behind the pattern forming process.

4 | DROPLETS

The controlled transport of electrically charged liquid droplets has important applications in controlled drug delivery and in the separation of micro/macro molecules [73–77]. Charged liquid droplets suspended in an immiscible fluid can be manipulated employing EFs [78]. This section presents a discussion on recent EK-based studies for the manipulation of liquid droplets.

4.1 | Electrophoretic patterning of droplets

Electrophoretic control of discrete droplets (EPDD) is a promising technique used for merging aqueous droplets through electrical interaction, also known as "electrocoalescence" [73]. In this technique, rapid charging of conductive droplets is used to achieve subsequent EP-induced motion. Recent studies have used EPDD for merging aqueous droplets and minimizing direct liquid-solid contact. A recent study by Kim et al. [74] reported the electrocoalescence and merging of droplets by employing a programmable digital microfluidics device. Their digital device consisted of two parallel electrode modules that enabled 3D programmable droplet handling. Figure 3A shows the horizontal and vertical transport of two microdroplets, electrocoalescence, and reciprocating droplet motions observed at 400 V applied between two pin electrodes separated by 2 mm. This study illustrates a versatile strategy for droplet manipulation that can enable biochemical and biomedical assessments that require the simultaneous handling of microdroplets.

Droplet electrocoalescence using EPDD was also employed by Peng et al. [73] to develop a digital microfluidic device powered by piezoelectric deflection caused by human finger movement. Their device had an array of piezoelectric elements, connected in parallel to metal electrodes, immersed in dielectric fluids. Finger motion caused deflection that was used to charge the piezoelectric elements and actuate the droplets across each electrode pair through EP force. This study demonstrated the electrocoalescence of aqueous droplets actuated at 200 V, as seen in Figure 3B, which shows the merging of a clear and a dyed droplet with and without a sustained electrode bias. Enhanced mixing was achieved by inducing internal flows in the droplet through continuous transportation of the droplet back and forth between the electrodes. In addition to droplet manipulation and mixing, EPDD can also be used for droplet transport. An important challenge in many microfluidic biomedical applications lies in the usage of bodily fluids that possess unpredictable and challenging sample characteristics such as high viscosities and extreme pH values. A potential solution to this limitation lies in the device by Peng et al. [73] that demonstrated the transport of both saliva and urine droplets. Figure 3C illustrates the transport of droplets of human urine (pH = 5.8) and saliva (pH = 6.4) by employing an actuation voltage of 200 V. This work provides an example of a portable, piezoelectrically powered EPDD device with potential applications in medical diagnostics.

4.2 | Dielectrophoretic patterning of droplets

Microfluidic systems are often prone to undesirable air bubbles being nucleated inside microchannels or inadvertently introduced when adding tubing connections to the devices [76, 79]. Air bubbles are highly undesirable, as they can affect device operation and generate parasitic heat transfer processes. Considerable efforts have

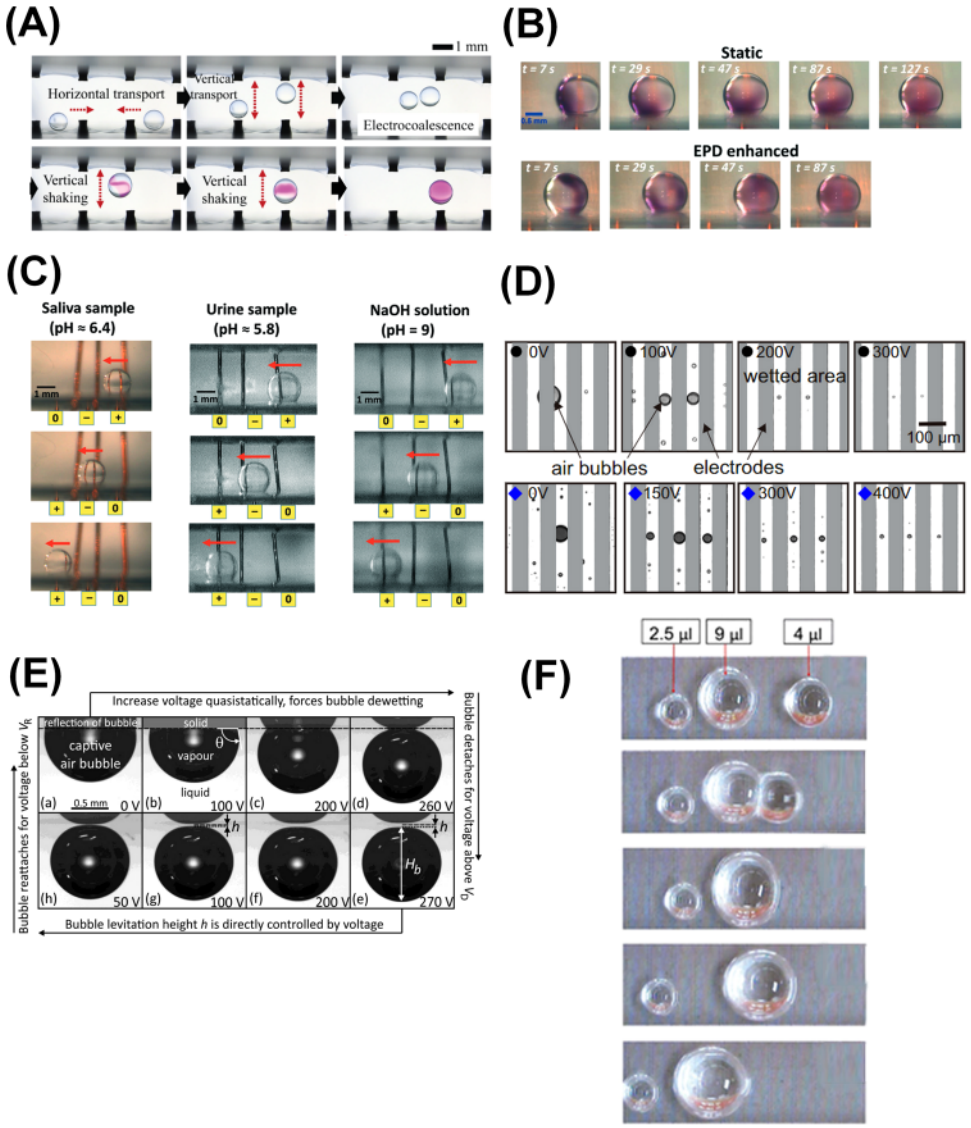

FIGURE 3 (A) Illustration of the merging of two oppositely charged microdroplets via electrical interaction and reciprocating motion. (B) Mixing of a clear and a dyed aqueous droplet by pure diffusion (top) and using electrophoretic control of discrete droplets (EPDD) actuation (bottom). (C) Sequential images (top to bottom) of a saliva droplet and urine droplet transported via finger powered microfluidic device. (D) Snapshots showing the elimination of bubble entrapment at different applied voltages using periodic dielectrophoresis (DEP) effect on ethanol droplets for two impact velocity values, 0.39 m/s (upper panel) and 0.91 m/s (lower panel), respectively. (E) Experimental images demonstrating DEP-based droplet manipulation via voltage-controlled bubble dewetting and detachment, levitation, and reattachment in a dielectric liquid. (F) Actuation of three deionized (DI) water droplets with different volumes (2.5, 4, and 9 µL) via liquid dielectrophoresis (L-DEP), where the droplets are taking to the left side for device disposal. *Source*: (A) Adapted from Ref. [74], open access article distributed under the Creative Commons Attribution (CC BY) License (2022). (B) Adapted with permission from Ref. [73], copyright (2016) Royal Society of Chemistry. (C) Adapted with permission from Ref. [73], copyright (2016) Royal Society of Chemistry. (D) Adapted from Ref. [77], open access article distributed under the Creative Commons Attribution (CC BY) License (2021). (E) Adapted from Ref. [76], open access article distributed under the Creative Commons Attribution (CC BY) License (2020). (F) Adapted from Ref. [75], open access article distributed under the Creative Commons Attribution (CC BY) License (2021).

been focused on developing DEP-based methods for the removal and subsequent transport of bubbles from surfaces. One of the most popular DEP-based techniques for this purpose is dielectrowetting or liquid dielectrophoresis (L-DEP), where the wetting behavior of a liquid on a solid surface is reversibly modified by DEP generated with a nonuniform EF. In a recent study, Vo and Tran [77] used DEP to deform the liquid surface when a droplet is sufficiently close to a solid surface. This process effectively induced controlled ruptures to the air film and created escaping tunnels for air. Entrapped air bubbles formed on the surface at applied voltages ranging from

0 to 400 V, as seen in Figure 3D. The entrapment of bubbles was observed to be manipulated by varying the applied voltage. At higher voltages, a large bubble (radius ~45 μm) experiences splitting of the air film and forms noticeably smaller bubbles along the electrode gaps. Bubble detachment, levitation, and reattachment using L-DEP were also demonstrated in the work by Brown et al. [76]. Successful bubble detachment and bubble levitation controlled by voltages ranging from 0 to 270 V are shown in Figure 3E. Captive bubbles were held indefinitely away from a solid surface with a programmable separation distance. These studies demonstrate that the effectiveness of DEP has for precise bubble elimination in microfluidic devices.

More recently, another interesting DEP-based actuation and manipulation of droplets to control their wetting behavior were reported by Frozanpoor et al. [75]. They developed a droplet-actuating platform by exploiting high EFs at the droplet solid–liquid interface using L-DEP. The actuation of deionized (DI) water droplets with different volumes (2.5–9.0 μL) at an actuation voltage of 85 V at 40 kHz using the iterative DEP approach are shown in Figure 3F. The main novelty of this work is the development of a droplet-actuating platform to control the wetting behavior of droplets and the properties at the droplet solid–liquid interface by introducing a lubricant layer and by controlling the L-DEP force. The actuation behavior was directed toward a cleaning application, resembling a scrubbing motion, while also transporting the droplets for disposal. This study offers an example of an energy-efficient droplet actuating platform to clean a variety of surfaces, a process with potential in the cleaning processes of automobile parts such as sensors, cameras, door mirrors, front side glass, and rear screen. It is expected that the next decade will bring programmable droplet actuating platforms for tackling cleaning issues, especially surface contamination in automobiles [80–82].

5 | SYNTHETIC PARTICLES

The development of rapid and straightforward methods for the manipulation and patterning of biological and synthetic particles on chips is a desirable capability in the development of biosensors [83], immunoassay devices [84], and tissue engineering systems [85]. These approaches benefit from the attractive features offered by miniaturization, such as short analysis time, reduced sample and reagent consumption, and better sensitivity [86]. Recent reports that employ EK mechanisms for the patterning of synthetic particles are discussed in the following subsections [43, 87, 88].

5.1 | Electrophoretic-based patterning of synthetic particles

EPD is a commonly used technique for the patterning of synthetic particles, as it offers superior control of the thickness, stoichiometry, and microstructure of the deposited layers than more traditionally approaches, such as hydrodynamic and magnetic forces [61]. This level of control is attained by adjusting both the magnitude of the applied voltage and treatment time [89]. Despite being a little over a century old, EPD is still a dynamic field, and exciting new developments are being made. In 2018, Mora et al. [90] reported a novel improvement called light-directed EPD (LDEPD). This technique involves the use of ultraviolet (UV) light that enables a localized control of an applied EF by using photo conductive electrodes [90]. In their work, the authors performed a three-step deposition of 70 nm tungsten, 300 nm alumina, and 150–190 nm polystyrene particles in three different patterns without using any sort of physical mask. Instead, a cell formed by titanium oxide and indium–titanium oxide (ITO) glass electrodes was energized with a +2 V DC bias voltage and UV light at a 100 mm distance from the emitting source for 90 s. This allowed for the patterning of the particles into simple geometrical shapes (a square, triangle, and circle) without requiring any hard tooling. Images of the patterns formed with this technique are shown in Figure 4A, where particle arrangement of into three distinct geometrical formations is observed. Although LDEPD can fully be automated, the patterning deposition was only possible when done at different times due to how the materials interact with the UV light. This limitation makes the simultaneous formation of distinct patterns a challenge to address in future LDEPD studies.

A possible solution to asynchronous treatment limitation in EPD was given in 2021 by Sopubekova et al. [91] with an EPD methodology capable of binary and successive patterning of silver, latex, and silica microparticles. Using chromium–gold electrodes fabricated by photolithography, the authors were able to deposit all three kinds of particles into the patterned structures using different voltages and treatment times. Silver particles, with sizes ranging from 80 to 100 nm using a 20 V DC bias voltage for 10 min, result in a deposition with 90% efficiency. Latex particles of 30 μm in diameter were also pattered alongside the electrode's structure with the same efficiency by applying a 15 V DC bias for 5 min. This decrease in the treatment conditions is attributed to the fact that latex particles presented a larger particle zeta potential magnitude (~70 mV) compared to silver particles (~60 mV). This is consistent with Equation (1); as latex particles have a greater zeta potential, they also possess greater v_{EP}, meaning that they

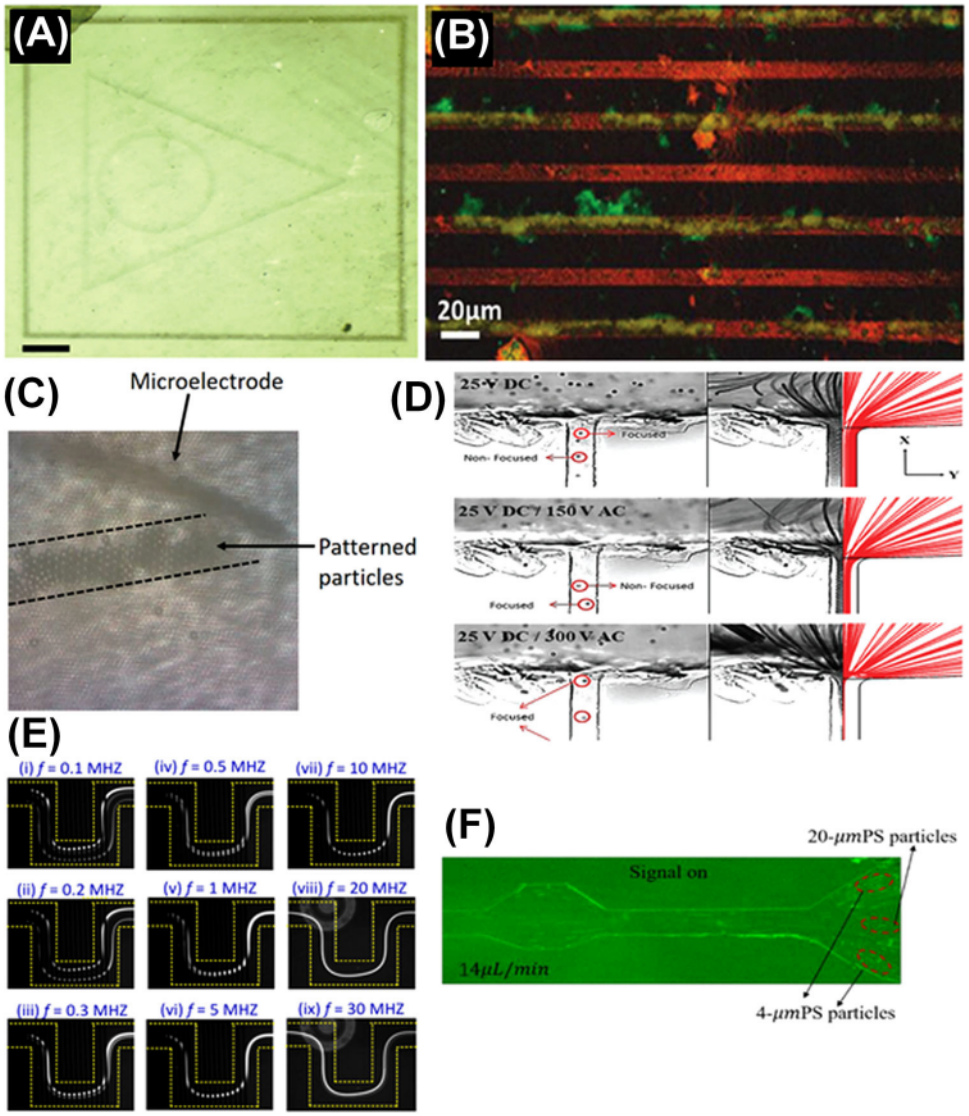

FIGURE 4 (A) Light-directed electrophoretic deposition (EPD) results demonstrating the reconfigurable deposition of alumina particles. (B) Superimposed image of latex (green) and silica (red) particles patterned on the same surface. (C) Line pattern of particles obtained after 30 s, on the lower surface of the silicon nitride (SiN) membrane by scanning the microelectrode (400 V_{pp}) horizontally at 10 μm/s. (D) Comparison of the experimental and predicted path-lines of 5 μm latex beads at the reservoir–microchannel junction of their device. (E) The fluorescent images of 13 μm polystyrene particle focusing streaks under different electric frequencies. $V_{pp} = 30$ V. (F) Image depicting the particle trajectory at 14 μL/min with 5 V signal applied. *Source*: Adapted with permission from Ref. [90], copyright (2018) Elsevier. (B) Adapted with permission from Ref. [91], copyright (2021) Springer Nature. (C) Adapted from Ref. [84], open access article distributed under the Creative Commons Attribution (CC BY) License (2019). (D) Adapted from Ref. [92], open access article distributed under the Creative Commons Attribution (CC BY) License (2018). (E) Adapted with permission from Ref. [93], copyright (2018) Elsevier. (F) Adapted from Ref. [94], open access article distributed under the Creative Commons Attribution (CC BY) License (2022).

are able to cover the same distance than the silver particles in a shorter time. Silica particles of 30-μm diameter were also treated with a 20 V DC bias for 5 min, resulting in the same deposition efficiency. A property unique to the silica particles was their noticeable tendency to deposit at the edges of the electrodes rather than at the center. This tendency is attributed to fringing field effects on the electrode edges. This unique property also allowed generating of silica/latex particle composites, with the former being deposited alongside the electrode edges and the latter occupying the middle regions. Successive patterning was done by submerging the electrode in an electrolyte solution containing silica particles, applying 15 V DC bias for 5 min, and then replacing the electrolyte solution to one containing latex particles without interrupting the voltage bias. This successive patterning of two different kinds of particles is shown in Figure 4B. The authors explicitly state that the methodology being used is applicable to any kind of

conductive electrode surface and any kind of material as long as it is electrically charged. The authors also stated that patterns of any shape can be formed and that the resolution is directly dependent on the dimensions of the electrode [91].

5.2 | Dielectrophoretic-based patterning of synthetic particles

Particle patterning and arrangement by rapid and simple manipulation have been demonstrated extensively using DEP [46, 95, 96]. Due to the unique ability of DEP to exert a force on both uncharged and charged particles, it has numerous applications in a wide array of fields, such as manipulation and assembly of micro components, the self-assembly of electronic devices, and, relevant to this review, microfluidic devices [97–100]. DEP-based manipulation has been extensively employed in the patterning, concentration, and separation of bioparticles [101, 102]. Although it was demonstrated that DEP can achieve higher order particle organization in porous membranes, there is still a research gap where particle arrangement at specific position on the porous membrane was not possible [84]. As a potential solution to address this limitation, Yasukawa et al. [84] demonstrated the positioning and patterning of polystyrene particles at a localized area on a silicon nitride (SiN) membrane with an array of 2-μm microholes by pDEP. As seen in Equations (3) and (4), when the f_{CM} has a positive value, the resulting $\mathbf{v}_{DEP}$ leads to pDEP. When an AC voltage was applied to a needle-type microelectrode, strong EFs were formed at the microholes of the SiN membrane in the region directly under the microelectrode, resulting in the particles moving toward the lower surface of the region. The movement of the microelectrode at 10 μm/s obtained with AC voltage resulted in microparticles patterning into a thick line formation along the trail of microelectrode movement. This was attributed to the shift of microholes by the strong EF, as seen in Figure 4C, which shows a line pattern of particles formed on the lower surface of the membrane at 400 V_{pp} with microelectrode motion at 10 μm/s. This method enables precise arranging particles at a desired position without requiring any templates or special electrode configurations. Through the unique capability to position particles at any location on membranes, this study provides a promising methodology for novel cocultivation systems and sensing platforms.

Another DEP-based study performed on latex beads was reported by Kale et al. [92, 103] where particle manipulation was enabled by EF gradients generated at the reservoir-microchannel junction. Their approach exploited the size difference between the inlet liquid reservoir and a microchannel, thereby eliminating the microfabrication of mechanical or electrical parts within the microchannel. Using latex beads as a proof of concept, they showed that a 3D reservoir–microchannel junction is crucial in enhancing the dielectrophoretic preconcentration potential of the devices. Their system, called reservoir-based dielectrophoresis (rDEP), resulted in a six-fold increase in the enrichment of latex beads and a significant reduction in the power consumption, which allows for a higher device integration [103]. Successful particle focusing was observed with an increase in AC voltage, and the beads were deflected to the channel centerline, as observed in Figure 4D obtained by applying a three voltage setting of 25 V DC, 25 V DC/150 V AC, and 25 V DC/300 V AC. Their work demonstrated that Joule heating effects can reduce rDEP particle focusing and could also potentially disable rDEP particle trapping. The authors attributed this effect to fluid temperature rise, which was indicated by electric current increase in the channel, which impacted particle velocity within the system. These findings provide means for integrating particle enrichment with downstream processes, for example, a detection system or a cell culture chamber in which the enriched target species would already be in a sedimented state to facilitate culturing.

5.3 | Hybrid systems employed for the patterning of particles

Though EP and DEP have been extensively used in particle patterning, deposition, and sorting, there are some drawbacks in employing these techniques such as the requirement of complex electrode designs and limited flexibility [104]. However, efficient particle patterning has been achieved by hybrid approaches that combine active external force fields with passive methods that depend on the microchannel structure and intrinsic hydrodynamic forces [93]. Hybrid systems that combine, for example, DEP with inertial forces [93, 94, 104], DEP with optically induced effects [104], and linear and non-linear EK [105] have shown promising results for electropatterning of micro/nanoparticles.

A major advantage of hybrid systems is their ability to tune and adapt to different particle samples once the microchannel structure and dimensions are fixed. Zhang et al. [93] demonstrated this capability using an innovative hybrid DEP-inertial microfluidic platform with three different sizes (4.8, 8, and 13 μm) of fluorescently-labeled polystyrene particles. The microfluidic device featured a sheath liquid flow to generate inertial forces, which combined with the DEP force induced by the bottom microelectrodes, resulted in effective microparticle focusing within the channel cross section. A unique aspect of

this platform is the capability for real-time tuning of the dimensions of the target binary particle mixture by adjustments to the electric voltage, without having redesigned the channel structure. Figure 4E illustrates the particle focusing streaks of 13 μm polystyrene particles obtained at an AC EF of 30 V_{pp} and frequencies ranging from 0.1 to 30 MHz. Their findings provided a superior alternative over other traditional inertial-based microfluidic platforms. Due to the high dependency on the sheath flow speed, the traditional microfluidic platforms can only be effective for specific range of target particles. However, when combined with DEP, as shown in this study, the DEP-inertial platform can provide real-time target tunability by simply adjusting the electric voltage. Another study that used the combination of EP and inertial forces was performed by Li et al. [94] with the development of a new cell sorting and separation method that combined 3D sidewall electrodes and contraction/expansion (CEA) structures. This system was used for the continuous flow separation of three types of particles: 4 μm polystyrene particles, 20 μm polystyrene particles, and 4 μm silica particles. The strategic interaction between electrophoretic forces and inertia forces enabled the separation. Due to inertial forces, sorting particles with different sizes was achieved in the CEA channel, as demonstrated in Figure 4F where it can be observed that the separation of 4 and 20 μm polystyrene particles was achieved at 14 μL/min at a potential of 5 V. The nonuniform EF generated in the 3D electrodes at the same height as the channels increased the action range of the DEP force. Their novel method of combining DEP and inertial forces achieved high precision sorting and separation of particles and cells.

A drawback of DEP technology is its limited flexibility in practical applications, mainly attributed to the requirement of complex electrode designs in traditional DEP systems [93]. An alternative is optically induced DEP (ODEP) [104], which uses virtual electrodes formed by illuminating optical patterns onto photoconductive layers with DEP to carry out micro/nano-object manipulation. The complex electrode manufacturing process is simplified by replacing the physical electrodes with virtual ones. This approach led to a shorter and simpler chip design cycle and lower processing costs. ODEP has been actively used to assemble and pattern polystyrene beads in recent years. Shi et al. [104] reported a model that solved an ODEP-based transient numerical model that simulated microparticles under AC EF coupling with an open flow field. The numerical results showed that particles with different conductivity could be separated with pDEP and nDEP effects caused by light illumination. The experimental results showed that the two DEP actions differentiated the conductive particle trajectories, enabling particle separation and patterning. Parameters such as the width of the bright area, applied AC voltage, and inlet flow velocity were optimized for efficient separation performance. Their study explained the mechanism behind the continuous particle manipulation was the combined action of AC EF and flow field. These findings unveiled the theoretical support behind the principles of particles continuous patterning and separation, opening the possibility for future device designs based on AC-ODEP technology.

6 | CELLS

The ability to form controlled arrangements of living cells is desirable in the fields of microfluidics and tissue engineering. Orderly formations of cells allow the interactions between neighboring cells to be studied, support localization of matrix molecules and soluble factors within the arrangement, and create more *in vivo* like environments [106, 107]. Electropatterning systems can configure cells at specific locations with resolutions down to the micrometer scale providing precise control over cell organization and interactions [108]. Both EP and DEP have been successfully employed to achieve the formation of 2D and 3D cell patterns for a variety of applications [109–111]; several recent studies reporting these findings are discussed in this section.

6.1 | Electrophoretic-based patterning of cells

The superior degree of control that EPD offers over more traditional deposition methodologies makes its applications to biological materials, such as cells, highly adaptable. A recent study by Brisson and Tilton [112] presented a method capable of the selective patterning of bacterial cells in a 2D arrangement. For these experiments, *Saccharomyces cerevisiae* cells were deposited onto a metallic electrode surface comprised of sodium bicarbonate ($NaHCO_3$). A cell concentration of 0.07% (w/v) was empirically determined to be below the number needed to form a complete monolayer on the surface. As such, any cell aggregation would be considered a direct result of the EF applications. The results seemed to indicate that there was no direct relation between the field frequency and the aggregate density; however, aggregate density was determined to be strongly dependent on the strength of the EF. Stronger AC voltages (>50 V) resulted in what the authors referred to as densely packed arrangements. On the other hand, lower intensity AC voltages (<50 V) resulted in loosely packed arrangements. An example of these "densely" and "loosely" packaged arrangements obtained using 10 Hz, 100 V and 10 V, respectively, is shown

in Figure 5A,B. This difference in packaging arrangement is solely attributed to the increased intensity of the EF. As can be seen in Equation (1), the electrophoretic velocity of particles is directly proportional to the EF magnitude. An increase in electrophoretic velocity would explain why cells would form denser arrangements under the same frequency and application time, as they would be moving faster at 100 V when compared to 10 V. The patterned arrays in this work were obtained without any chemical modification of the target surface, which was a limiting factor in the previous EPD research related to cells.

Yet another interesting development in the field of EPD with cells was reported by Neirinck et al. [113], where both living *Staphylococcus aureus* and *Escherichia coli* were deposited on a stainless steel surface. The purpose of this work was to measure cell viability of two industry-relevant bacterial cells in the context of continuously stirred tank reactors. The authors aimed to prove that EPD was an effective method to generate biofilms while maintaining cell viability within an acceptable margin. Deposition was done using two suspending solutions, a sucrose suspension and demineralized water, with the latter obtaining the most promising results. The deposition of both *S. aureus* and *E. coli* after 2400 s of applying 100 V_{pp} at 25 Hz is shown in Figure 5C,D. As can be seen, the vast majority of cells remain alive after the treatment with the EF, suggesting that the treatment conditions have no significant impact on cell viability. It is also noticeable that *S. aureus* had better deposition than *E. coli*; the authors attribute this to the difference in conductivity between the two cell lines. *S. aureus* presented a conductivity of ~50 μS/cm, whereas *E. coli* only reached ~38 μS/cm. Regardless, the experiments appeared to have yielded positive results and both bacterial cell populations could be deposited into metallic surfaces without significantly affecting their viability.

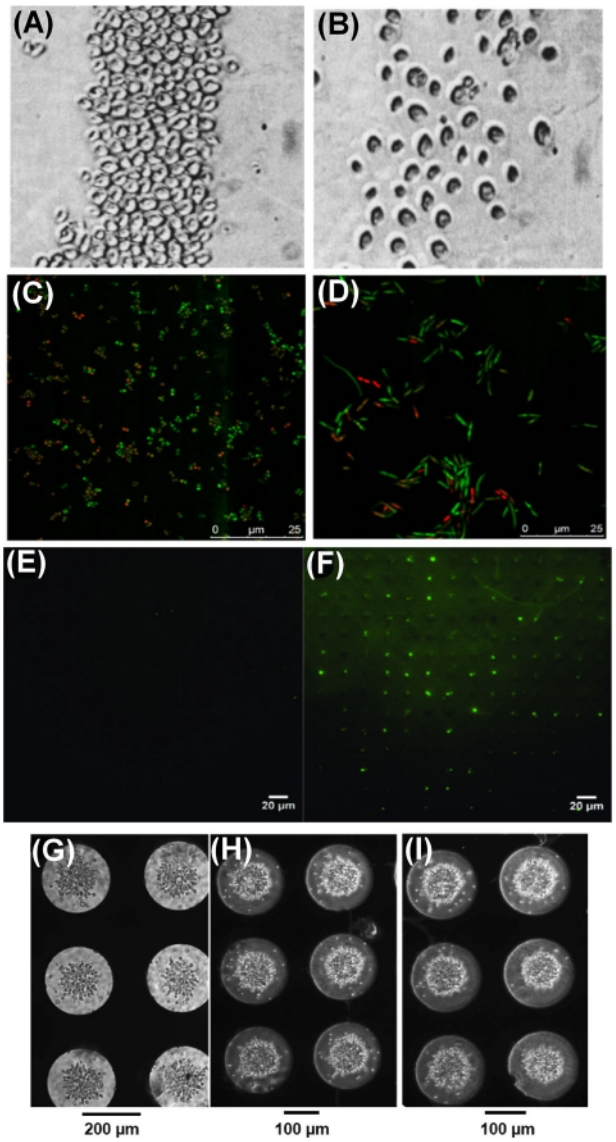

FIGURE 5 (A) Densely and (B) loosely packed *Saccharomyces cerevisiae* cell clusters in different regions of the same $NaHCO_3$ surface. (C) *Staphylococcus aureus* and (D) *Escherichia coli* cells after a 2400-s deposition process at the electrode from a demineralized water solution. Living cells were stained in green, whereas the dead cells are red. (E) Collection of *Salmonella typhi* cells before and (F) after application of a 20 V_{pp} and 5 MHz electric field for 1 h. (G) Obtained cell aggregation using the dielectrophoresis (DEP) dot electrode system for K562 cells in polyethylene glycol (PEG)-DA gel, (H) yeast cells in 6.75% v/v collagen, and (I) yeast cells in 25% PuraMatrix gel. *Source*: (A) and (B) Adapted with permission from Ref. [112], copyright (2001) John Wiley and Sons. (C) and (D) Adapted with permission from Ref. [113], copyright (2009) Elsevier. (E) and (F) Adapted with permission from Ref. [114], copyright (2018) Elsevier. (G)–(I) Adapted from [115], open access article distributed under the Creative Commons Attribution (CC BY) License (2020).

6.2 | Dielectrophoretic-based patterning of cells

Over the last few decades, DEP has garnered considerable interest in biological analysis. This interest is mainly due to its relatively short response time, precise and easy operation, and low degree of cell damage [47]. Another major advantage DEP presents as a methodology for studying cellular systems is that it is label-free, which trivializes the difficulty of finding an assay marker that does not interact with the model organism [116, 117]. The differing EK properties between the membranes of different cells allow DEP to be used as a highly tunable technique for the manipulation of bioparticles. Examples of this manipulation include the selective trapping of cells according to their species [118], the structured arrangement of different

kinds of microbial cells to a surface [119, 120], the controlled formation of cell aggregates with defined size and shape [121, 122], among others.

Despite its attractive characteristics, the spatially controlled assembly of live bacterial cells employing DEP remains mostly unexplored. Due to this apparent gap in knowledge, Goel et al. [114] developed a methodology capable of patterning two different bacterial cells. In this research work, the authors demonstrated the dynamic patterning of two live, pathogenic Gram-negative bacteria, *Salmonella typhi* and *E. coli*, respectively. This work aimed to collect bacterial cell inside microwells to discern among different types of bacteria within two-population mixtures. Cell suspensions were subjected to varying nonuniform AC EFs applied through microelectrode arrays resulting in the slow collection of bacteria in the microwells. The process was fully reversible; the electrodes could be restored to their initial state within minutes of turning off the EF. Hence, each device was expected to withstand at least 50 trials of these kinds of experiments. The EF application time was empirically selected to be 15 min, as this allowed a high enough number of cells to draw sensible inferences on the results without clogging the device. The results yielded by these experiments showed that for assembly to occur, 10 V_{pp} and 50 kHz were the minimum requirements for cells to assemble. Lower frequencies and V_{pp} values resulted in the cells not showing any effect to the EF application. The best cell assembly results were obtained at a voltage of 20 V_{pp} and 5 MHz, experimental images of the collection of *S. typhi* cells under these conditions are shown in Figure 5E,F. The highest frequency at which cells experienced pDEP was determined to be 20 MHz, which lies above the experimental system limits of the described experimental setup. The overall reported cell collection efficiency for a bulk concentration of 10^5 cells/mL was estimated to be around 90%. Of the collected cells, 96% were viable at the end of the 60 min experimental process [114].

It is worth noting that most bacterial cells are more resistant to external stresses than eukaryotic cells [123]. Thus, the assumption that a particular methodology would yield the same degree of viability using the two different types of cells is incorrect. To this end, Henslee et al. [115] used DEP-capable dot electrodes to form 3D cellular structures, with promising results using yeast, HL-1, K562, and HeLa cells. This work aimed to answer two questions: (1) Does DEP manipulation has a negative impact on cell viability? (2) Is there a significant difference in cell viability between 2D and 3D cell structures? To measure cell viability, the cell aggregates were subjected to two distinct drugs: Vinblastine and Amphotericin B. Dot electrodes were used to contain cells via nDEP, which caused repulsion from the edges of the electrode patterns and forced cells into aggregates. The resulting cell aggregates, obtained at 10 V_{pp} at 10 kHz, can be observed in Figure 5G–I. Given that the cell lines used in this work were of similar size (~10 μm in radius), the resulting aggregates also presented similarities in size. The authors pointed to these finding as evidence of successfully producing homogenous aggregates. To properly verify the effect of DEP-based 3D cell culture on cells, the authors investigated the properties of the studied cells after DEP treatment. The electrophysiological properties of cells grown in 2D were determined for 24 and 48 h and were compared to those produced in 3D for the same time periods. Data analysis revealed a significant change in the membrane capacitance for HeLa cells after 3D encapsulation compared to their 2D counterparts. Membrane conductance for yeast and K562 cells also demonstrated a significant change, which was assumed to be due to the 3D enclosing. It is worth mentioning that in the case of yeast cells, the changes in membrane conductance were only observable at 24 h. This fact seemingly implies that at least for that cell line, changes in electrophysiological properties were only temporary.

7 | GELS

Gels are an increasingly popular material for 3D cell cultures due to their biological and mechanical properties [124–126]. Gels are 3D networks able to assimilate large amounts of water and/or biological fluids, making them excellent options for applications that require a resemblance to biological tissue [67, 127–129]. Recent reports on the formation of patterns in gels using EK mechanisms are discussed in the following sections.

7.1 | Electrophoretic-based patterning of gels

Since the early 2000s, there has been an increased interest in developing 2D surfaces with molecular arrangements by photolithography and microfluidic approaches [130–132]. However, their functionality and effectiveness are severely limited by the inability to create an accurate representation of the 3D natural cellular environment [133–135]. Although a vast number of fabrication methodologies exist for 3D gel environments, most possess notable disadvantages hindering the possibility of widespread usage. These disadvantages include the use of UV radiation [136], limitations in the capacity to pattern large or complex molecules [137], and expensive processes or chemical reactions [138]. In recent years, the usage of EFs to achieve 3D patterning of gels has increased, as these simple and affordable systems allow the localization of molecules within the gel network [139–141].

A recent example of the formation of 3D gel environments lies in the work by Aguilar et al. [142], where they reported the combination of EP with hydrogel photopolymerization for the patterning of NIH-3T3 cells. They developed a platform called "3D electrophoresis-assisted lithography" (3DEAL), which created molecular patterns of different sizes, geometry, and composition. This platform used EP to manipulate fibronectin (FN) molecules independently of charge and size and localize them within the hydrogel. The described system is composed of five elements: power supply, platinum electrodes, buffer reservoirs, hydrogel compartment, and tubing connections. This process used EP to drag the "printing" molecules along the direction of the EF, which generated both the size and shape of the desired pattern within the gel network. Given the capability of the 3DEAL system to pattern multiple types of hydrogels with numerous types of proteins, it offers an alternative to generate hydrogels with anisotropic chemical compositions that can be selectively recognized by cells. To evaluate this possibility, a polyacrylamide–collagen (PA–Colla) gel with circular columns of FN that were 150 μm wide in diameter and 800 μm in depth was patterned. Immunofluorescent microscopy images of the resulting pattern obtained at 150 V are shown in Figure 6A. Although the 3DEAL methodology generated patterns that could theoretically allow cells to migrate up to 800 μm in depth into the hydrogel network, cells did not penetrate beyond ~100 μm. The authors theorized that this limitation in movement can be attributed to the low porosity of the PA–Colla gel, which may affect cell and oxygen diffusion. These results seemingly demonstrated the capacity of the 3DEAL system for the generation of hydrogel environments with functional macromolecules. This platform serves as an example of a simple and accessible method to create anisotropic environments using hydrogel pattern generation.

Another recent EP-based study by Gargava et al. [143] demonstrated the use of EFs to rapidly form alginate (Alg) gels in specific 3D patterns. Gel synthesis starts with an agarose, a thermoresponsive biopolymer, which was previously loaded with Ca^{2+} ions (0.1 wt% of $CaCl_2$) and placed in a beaker. The inner surface of the beaker was wrapped with aluminum foil, which acted as a cathode, and copper wire, which served as an anode. When a potential of ~10 V was applied with a DC power source, an Alg gel formed, having the shape of the mold. Gelation occurred due to the Ca^{2+} ions electrophoretically migrating away from the mold, at which point they crosslinked with the Alg chains. An overview of this methodology and a fluorescence micrograph of the obtained polymer are shown in Figure 6B. The main advantage of this technique was that it provided a framework for manufacturing 3D gel networks without using any additional instruments.

7.2 | Dielectrophoretic-based patterning of gels

As DEP does not depend on electrical charge to achieve the manipulation of molecules or particles, it is the technique of choice when handling uncharged materials. An example of these important dielectric materials is polyethylene glycol (PEG). PEG-based hydrogels show high antifouling properties, mainly attributed to their neutral charge and absence of hydrogen bond donors [144]. These attractive characteristics have enabled the use of PEG-based hydrogels sensors in clinical trials [145–147]. Kim et al. [148] spatially immobilized beta amyloids 1–40 and 1–42 ($A\beta_{1-40}$ and $A\beta_{1-42}$) within a PEG gel network to create a sensor to diagnose Alzheimer's disease. Their work aimed to demonstrate the feasibility of plasma-based Alzheimer's diagnosis by combining the properties of PEG-based hydrogels with DEP forces. The sensor was based on a spiral microelectrode (SME) structure covered with a hydrogel with a specific pore size and thickness, onto which fragmented antibodies were immobilized. A visual representation of the immobilized $A\beta_{1-40}$ and $A\beta_{1-42}$ antibodies can be seen in Figure 6C. Both antibodies are mostly confined to the bounds set by the hydrogel network and concentrated to the bottom of the gel, where the sensor is located. The switching between pDEP and nDEP forces is achievable by a change in the relative polarizability, which is denoted as a change in the sign of the f_{CM} in Equation (4). This variation in the sign of the f_{CM} is the result of varying the applied field frequency. The frequency conditions for pDEP and nDEP were 1 kHz and 100 MHz, respectively. The dynamic capability of switching between pDEP and nDEP in tandem further concentrated the amyloids and removed the nonspecific plasma proteins, improving the density of immobilized fragmented antibodies within the sensor region. The SME sensor could quantify disease-related proteins of known sizes with high sensitivity, providing high utility for diagnosing multiple diseases besides Alzheimer's at its earlier stages. This SME sensor could represent a significant leap in plasma-based disease diagnosis with high accessibility and affordability.

8 | CONCLUSIONS

This article aims to provide an overview of the current advancements in the development of miniaturized systems for electropatterning particles, ranging in size from colloids to gels. The recent findings by the several research groups reported in this review support the fact that EK phenomena have been successfully used for the efficient and accurate arrangement of a wide range of particles

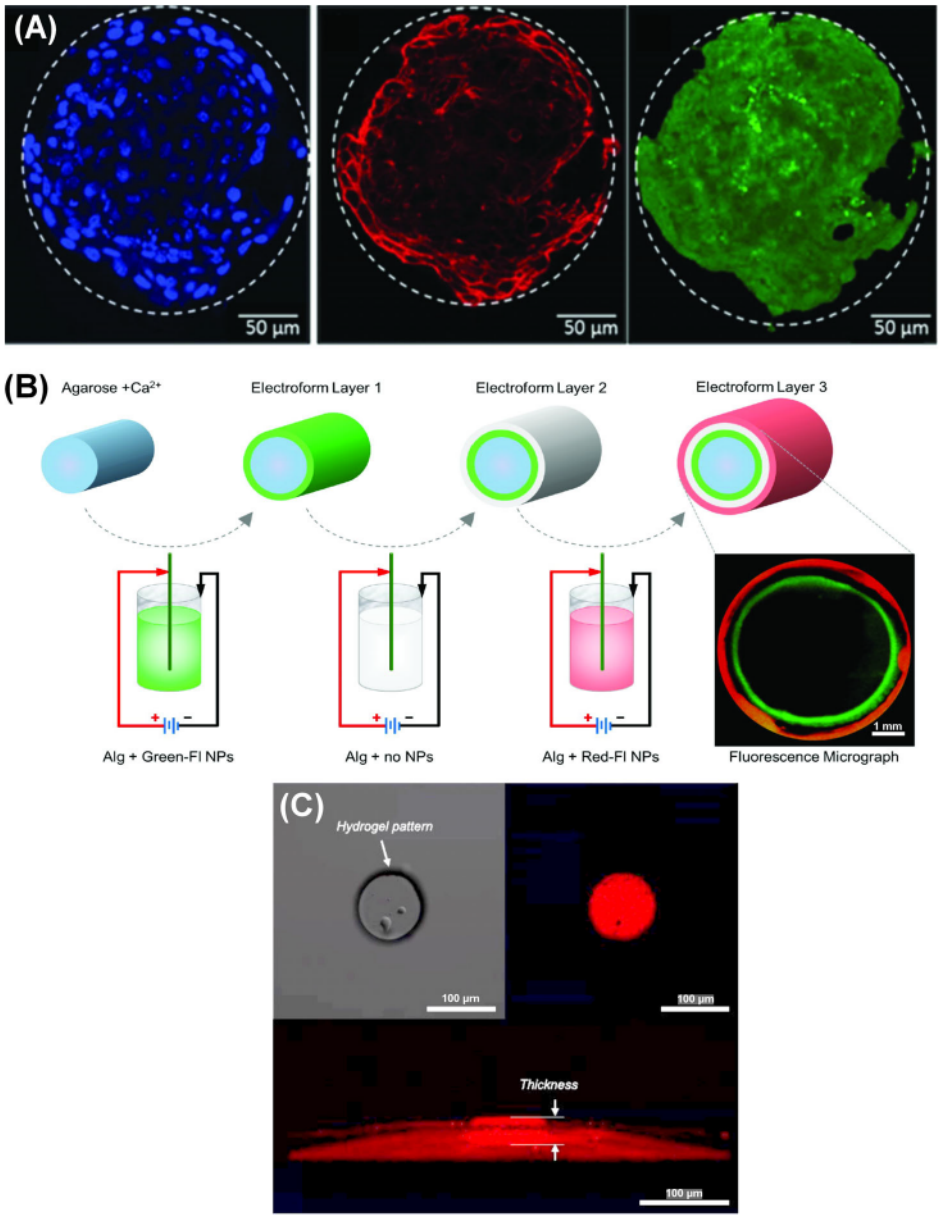

FIGURE 6 (A) Immunofluorescent microscopy images of a cell cluster showing the cell nuclei (blue) and actin cytoskeleton (red) directly on the 200 µm diameter fFN + fibronectin (FN) pattern (green). (B) Electroformation of multiple, distinct alginate (Alg) gel layers concentrically around an agarose core. The Ca^{2+} containing cylindrical agarose mold is coated with successive layers of Alg gels containing green-fluorescent nanoparticles, followed by a fluorescence micrograph of the tube cross section showing the final structure's multiple layers. (C) Measurement of the polyethylene glycol (PEG)-hydrogel thickness labeled employing confocal microscopy. Shown in red are both $A\beta_{1-40}$ and $A\beta_{1-42}$ dyed using TAMRA. Both antibodies are mostly confined within the hydrogel structure and localized at the bottom of the gel network, where the sensor is located. *Source*: (A) Adapted with permission from Ref. [142], copyright (2018) John Wiley and Sons. (B) Adapted with permission from Ref. [143], copyright (2021) American Chemical Society (ACS). (C) Adapted with permission from [143], copyright (2019) Elsevier.

of interest. Although many of the reports here employed either EP or DEP, some of the cited examples combine EK techniques with other methodologies to improve the characteristics particle patterning. Section 2 of the present review included a discussion of the fundamentals behind the phenomena of EP and DEP. This discussion also aimed to provide more context on the results presented by the covered articles and explain why some parameters are of particular importance, such as voltage in EP works and frequency in DEP works.

Sections 3–7 of this review of contemporary research on electropatterning are ordered in terms of their size and structural complexity, starting with simple colloidal arrays and ending with complex 3D gel networks. Although most

TABLE 1 Summary of the material properties, operating conditions, and key findings of the electropatterning techniques discussed in this review separated by particle of interest.

Category	Technique used	Material properties	Operating conditions	Key findings	Refs.
Colloids	EP	Patterned material: Ag_2O_2 cuboids Size: 100–400 nm diagonal size	Experimental conditions: constant current mode with current density of 100 μA/cm^2 Electrode material: silicon wafer (anode) and silicon wafer covered with gold film (cathode)	• A new growth mechanism during EPD of silver colloids in constant current mode was revealed • The colloid formation mechanism was ascribed to electrochemical oxidation and oriented attachment growth of silver nanoparticles during EPD • Deepened the understanding of physical and chemical processes during EPD	[59]
		Patterned material: SiO_2–SiO_2 composite particles Average size: 200 nm and 16 μm	Experimental conditions: a sequence of AC (5 V with a frequency of 1 Hz) and DC (5 V) EF stimulation Electrode material: Conductive tapes	• Formation of 2D and 3D, close packed arrays by EP stimulation with DC and AC EFs was achieved • Bottom-up stacking of the ordered arrays was observed during EP stimulation process using AC EF	[58]
		Patterned material: Fluorescent carboxylate particles of 1–3 μm diameter and 3 μm plain polystyrene particles	Experimental conditions: EF generated with an amplitude of 80 kV/m and frequencies ranging from 50 Hz to 10 kHz Electrode material: Metal needles	• Predominant effect on wall repulsion of charged colloidal particles in microfluidic channels was investigated and analyzed • At high frequencies, DEP was demonstrated to be the main mechanism for wall repulsion • The most significant wall repulsion was exhibited at lower frequencies, where the major contributing force to the wall repulsion was hydrodynamic flows	[57]
	DEP	Patterned material: Janus particles and polystyrene particles Average particle sizes: 3, 5, 10 and 15 μm in diameter for Janus particles 100, 300, 520, 720 and 1000 nm average size for polystyrene particles	Experimental conditions: AC EF ranging between 10 and 14 V at frequency of 100 kHz Electrode material: ITO coated glass	• The tasks of loading multiple nano/micro-sized targets and driving their transport were unified • The need for pre-labeling or surface modification of the cargo was eliminated • Selectively loading/unloading and dynamic variation of the cargo was achieved by simply changing the frequency of the applied field	[62]
		Patterned material: Blue, red and yellow polystyrene microspheres in water Average particle diameters: Blue (7 μm), yellow (4 μm) and red (7 μm)	Experimental conditions: Increasing AC EF ranging between 0 and 130 V_{pp} at fixed frequency of 300 kHz Electrode material: ITO coated glass	• Development and validation of an eMAP to construct and manipulate 3D colloidal assemblies within water droplets based on DEP was reported • Four main distinct 3D colloidal assemblies within water droplets (bottom base, wing-like, rising-chain-like and top-cap-like) were created by tuning the applied AC signals, colloidal properties and droplet size	[63]

(Continues)

TABLE 1 (Continued)

Category	Technique used	Material properties	Operating conditions	Key findings	Refs.
	Hybrid	Patterned material: Polystyrene particles Average particle size: 700 nm in diameter	Experimental conditions: Sequence of 10 dc pulses of 1.5 mA over 0.5 s with a 10 s off period between pulses Electrode material: ITO coated glass	• Robustness of a colloidal coating process was investigated by systematically combining AC and DC EF application • 2D, non-closed packed colloidal arrays were first obtained by application of low frequency AC field application • Fixing of the particle array onto the substrate to keep it intact after field removal and solvent evaporation was achieved by a sequence of DC pulses	[64]
		Patterned material: AuNP suspensions Average particle size: 17 nm for obtaining film and 10 μm for obtaining microwire	Experimental conditions: AC EF with 20 V_{pp}, 100 Hz for 5 min Electrode material: ITO coated glass	• Scaling of the AC-DEP force with both particle size and field frequency in such a way that DEP becomes the dominant effect beyond a critical particle diameter (6 μm for AuNPs at 100–500 Hz) was observed • Colloidal structures transition from films to microwires as the NP diameters increase from nanometers to micrometers, with no observable assembly at intermediate NP sizes • The film formation was purely governed by surface EHD, whereas the microwire synthesis was an EHD-assisted-DEP process	[51]
		Patterned material: coacervates and coffee Average particle size: 1.2 μm mean diameter	Experimental conditions: AC EF with 17 mV/μm, 500 Hz for 100 s Electrode material: metal electrodes	• Band and zigzag patterns of suspended microparticles subjected to AC EFs were experimentally demonstrated • The physical mechanisms underlying the pattern formation process of colloids in aqueous suspension subjected to AC EFs were identified as dipole–dipole interactions and second order EK fluid flow	[65]
Droplets	EP	Patterned material: Droplets of NaOH, PHP and silicone oil Average droplet size: 0.72 mm in diameter	Experimental conditions: Applied voltages are 200, 300 and 400 V Electrode material: Pin socket-based electrode array	• Electrocoalescence and merging of droplets employing a programmable digital microfluidics device was investigated • The different types of programmable 3D droplet handling which were demonstrated using the platform include horizontal and vertical transport of two oppositely charged microdroplets, and horizontal and vertical reciprocating motions of the droplets	[74]
		Patterned material: Different kinds of aqueous droplets like DI water, human body fluids (saliva and urine) and NaOH Average droplet size: Droplet radius ranging from 0.2 to 1 mm	Experimental conditions: Applied voltage for actuation is 200 V Electrode material: Pair of piezoelectric elements	• Development of a finger-powered digital microfluidic device based on the EP transport of discrete droplets was reported • Merging of aqueous droplets with and without sustained electrode bias was experimentally observed • The transport of droplets of human urine (pH = 5.8) and saliva (pH = 6.4) was achieved by employing an actuation voltage of 200 V	[73]

(Continues)

TABLE 1 (Continued)

Category	Technique used	Material properties	Operating conditions	Key findings	Refs.
	DEP	Patterned material: entrapped bubbles generated by ethanol droplets Average droplet size: droplet radius of 1.3 mm	Experimental conditions: DC voltage varying from 0 to 400 V Electrode material: interdigital array of gold electrodes	• Deformation of the liquid surface of a droplet when it is sufficiently close to a solid surface to induce controlled ruptures to the air film and create escaping tunnels for air was induced by using DEP effects • The entrapped air bubbles formed on the surface were manipulated by increasing the applied voltage • Effective minimization of bubble entrapment and splash formation using DEP was theoretically and experimentally demonstrated	[77]
		Patterned material: air bubbles Average droplet size: bubble volumes were in the range of 0.4–2.4 μL	Experimental conditions: DC voltage varying from 0 to 270 V Electrode material: titanium–gold interdigitated microstripe electrode array	• DEP controlled bubble detachment, levitation, and reattachment, applicable for dielectric and conducting liquids was shown • Dewetting and detachment of a vapor-filled bubble from a solid surface was observed when the voltage exceeded a critical value • The geometry of the system was shown to play a key role in determining the detachment and reattachment touchdown voltages	[76]
		Patterned material: DI water droplets Average droplet size: volumes were in the range of 2.5, 4, and 9 μL	Experimental conditions: DC voltage varying from 20 to 100 V Electrode material: patterned aluminum electrodes on glass substrate	• A droplet actuating platform to control the wetting behavior of water droplets by exploiting high EFs at the droplet solid–liquid interface using L-DEP was presented • Reduction of the operating voltages for L-DEP was achieved by exploiting the high EFs at the droplet solid–liquid interface and by introducing a lubricant layer	[75]
Synthetic particles	EPD	Patterned material: Alumina Size: 150–190 nm in diameter	Experimental conditions: +2 V DC bias and UV light Electrode material: ITO and fluorine-doped tin oxide (FTO) glass	• Particle arrangement of three distinct geometrical formations (square, triangle and circle) was achieved • The deposition was only possible when done at different times due to how the materials interact with UV light	[90]
		Patterned material: Silver, latex, and silica Size: 80–100, 30, and 30 nm respectively	Experimental conditions: 15 and 20 V DC bias Electrode material: chromium and gold	• Precision in depositions on metallic surfaces was observed to increase along applied EF magnitude • As ζ potential of the solution gets higher, particles got deposited faster • Pattern resolution is dependent solely on electrode dimensions	[91]

(Continues)

TABLE 1 (Continued)

Category	Technique used	Material properties	Operating conditions	Key findings	Refs.
	DEP	Patterned material: water and suspension of polystyrene particles Average particle size: 3 and 10 μm diameter	Experimental conditions: AC voltage with 400 or 500 V_{pp} at 1 kHz frequency Electrode material: ITO electrode and needle-type Pt microdisk electrode	• Positioning and patterning of microparticles at a localized area on an SiN membrane was demonstrated by pDEP • A line pattern of particles was obtained along the trail of a moving microelectrode using AC voltage application	[84]
		Patterned material: latex beads Average particle size: 5 μm diameter	Experimental conditions: three voltage settings of 25 V DC, 25 V DC/150 V AC, and 25 V DC/300 V AC Electrode material: platinum electrodes of 0.5 mm diameter	• Particle and cell manipulations using rDEP was demonstrated by tuning the naturally produced EF gradients at the reservoir–microchannel junction • An increase in particle focusing was observed with an increase in AC voltage • A sixfold increase in the ability to focus particles using a 3DrDEP device over its 2DrDEP counterpart for a given applied voltage was shown by the quantification of the focusing effectiveness	[103]
	Hybrid	Patterned material: Polystyrene particles Average particle size: 4.8, 8 and 13 μm average diameters	Experimental conditions: AC EF of 30 V_{pp} and different frequencies ranging from 0.1 to 30 MHz Electrode material: Patterned microelectrodes	• A hybrid DEP-inertial microfluidic platform combining inertial and DEP forces to focus particles of three different sizes was demonstrated • Variation to the dimension of target particle mixture was achieved by adjusting the electrical voltage, thereby eliminating the need to redesign the channel structure or dimensions	[93]
		Patterned material: polystyrene and silica particles Average particle size: 4 and 20 μm polystyrene particles, and 4 μm silica particles	Experimental conditions: 5 V applied DC signal Electrode material: 3D electrode structure with Ag-PDMS electrodes	• A sorting and separation method for three different kinds of particles was developed by utilizing the combination of EP and inertial forces • A contraction/expansion electrode setup was developed with a capability to sort particles of different sizes due to inertial forces and to enhance nonuniformity of the applied EF • High separating efficiency ranging from 92.1% to 95.3% was achieved for both numerical simulations and experimental observations	[94]
Cells	EPD	Patterned material: *S. cerevisiae* cells	Experimental conditions: 10 and 100 V AC voltage, 10 Hz frequency Electrode material: gold	• Surface chemical templating of the substratum is not required to produce arrays or patterns • Dense 2D cell clusters were formed in minutes from extremely dilute (0.03% and 0.07% w/v) cell suspensions • The formed arrays are reversible and dissipate by diffusion on removal of the EF	[112]

(Continues)

TABLE 1 (Continued)

Category	Technique used	Material properties	Operating conditions	Key findings	Refs.
		Patterned material: *Staphylococcus aureus* and *Escherichia coli* cells	Experimental conditions: 100 V_{pp} and 25 Hz frequency Electrode material: stainless steel foiled polystyrene cuvettes	• Significantly higher conductivity was consistently measured for both cell types in the demineralized water suspensions • Higher currents during deposition resulted in a drastic reduction of living cells in the deposit • The degree of cell death is much lower than that of previous reported literature for pulsed DC currents applied for the same duration	[113]
	DEP	Patterned material: *Salmonella typhi* and *E. coli* cells	Experimental conditions: 100 V_{pp} and 25 Hz frequency Electrode material: ITO glass	• Voltage and frequency were optimized to for maximum cell capture, which gave an entrapment efficiency of 90% in 60 min	[114]
		Patterned material: using yeast, HL-1, K562, and HeLa cells Size: 100–150 μm	Experimental conditions: 20 V_{pp} and 5 MHz frequency Electrode material: ITO glass	• Both 2D and 3D cell arrangements were formed • There was a significant change in the membrane capacitance for cells after 3D encapsulation when compared to their 2D counterparts • For one cell type (yeast) the changes in membrane conductance were only observable at 24 h. Changes in electrophysiological properties were only temporary	[115]
Gels	EP	Patterned material: PA–Colla gel	Experimental conditions: 150–200 V Electrode material: platinum	• EP was used to move functional molecules and localize them within hydrogels with high degrees of precision • The limitation in cell movement was attributed to the low porosity of the PA–Colla gel, which may affect cell, and oxygen diffusion	[142]
		Patterned material: alginate (Alg) gel	Experimental conditions: 20 V Electrode material: graphite and aluminum	• Gelation occurred due to the calcium (Ca^{2+}) ions electrophoretically migrating away from the mold • This technique provided a framework for manufacturing 3D gel networks without usage of 3D printer	[143]
	DEP	Patterned material: polyethylene glycol (PEG)	Experimental conditions: 0.5 V and 20 MHz frequency Electrode material: tantalum/platinum	• The $A\beta_{1-40}$ and $A\beta_{1-42}$ antibodies were immobilized within a PEG gel network to create a sensor to diagnose Alzheimer's disease • Both antibodies can be seen being confined to the bounds set by the hydrogel network • The switching between pDEP and nDEP forces in tandem further concentrated the antibodies and removed the nonspecific plasma proteins	[148]

Abbreviations: AC, alternating current; DC, direct current; DI, deionized; DEP, dielectrophoresis; EF, electric field; EHD, electrohydrodynamic; EK, electrokinetic; eMAP, electro-microfluidic assembly platform; EP, electrophoresis; EPD, electrophoretic deposition; ITO, indium–titanium oxide; L-DEP, liquid dielectrophoresis; nDEP, negative-DEP; PA–Colla, polyacrylamide–collagen; pDEP, positive-DEP; PEG, polyethylene glycol; rDEP, reservoir-based dielectrophoresis, *S. cerevisiae*, *Saccharomyces cerevisiae*; SiN, silicon nitride; UV, ultraviolet.

of the cited works differed vastly in terms of their particle of interest and intended field of application, some interesting commonalities are found within each technique. Studies that made use of EP for the manipulation of particles relied mostly on AC EFs when they required a denser packaging or the formation of a more complex 3D structure. This is mainly due to the added advantage of high tunability of particle pattern formation that is superior in AC fields when compared to DC ones. For the case of works that used DEP for particle manipulation, most combined it in tandem with other techniques to achieve better results, such employing both pDEP and nDEP in tandem. This is mainly due to the high degree of tunability that this technique intrinsically possesses. A summary of Table 1 lists the experimental conditions as well as the main findings of each of the studies analyzed in this review.

Most of the studies included in this review article that employ EP as the main manipulating force use AC fields, whereas only a few use DC EFs as a bias for the AC signal. The reason why AC signals are preferred is because they provide a higher control of the particles being manipulated by tuning parameters such as amplitude and frequency. Recent reports use EP mostly for the manipulation of inorganic materials as these have an inherent electrical charge. The simultaneous manipulation of particles of different materials for the formation of distinct patterns is a limitation of EP-based techniques. Despite recent efforts being made, this is still a significant challenge to address in most EP-based systems. In recent years, DEP has become the most prevalent EK method for manipulating organic particles; this because DEP does not require the object to have an inherent electrical charge. Another advantage that DEP has is its enhanced capability for the formation of complex 3D structures that are of particular importance as they serve as a better representation of *in vivo* systems than 2D arrangements. Manipulation by means of DEP has the advantage of being label-free, which makes it attractive for clinical or biomedical applications. Although the results presented in DEP-based studies are promising as a proof-of-concept, this technology has little commercial presence. More efforts are needed for DEP to be accepted by the widespread market. An additional advantage EK-based methodologies is their ease of integration with other phenomena as discussed in the previous sections. Due to the flexibility provided by hybrid approaches, it is expected that the combination of multiple manipulation mechanisms will become more popular in the future. We optimistically foresee that EK-based manipulation techniques, both individually and in combination with other techniques, will exhibit great potential in generating novel advancements in the field of pattern generation in microfluidics.

ACKNOWLEDGMENTS

This work was partially supported by the NIH under award numbers R21GM143658 and R16GM146687; and NSF awards 2150798 and 2127592. The content is solely the responsibility of the authors and does not necessarily represent the official views of the funding agencies. The authors thank the members of the Biological Microsystems and the Microscale Bioseparations laboratories at RIT for their insightful thoughts and scientific discussions. The authors also thank Joanne Park for her valuable contribution in the creation of Figure 1A of this manuscript.

CONFLICT OF INTEREST STATEMENT

The authors have declared no conflict of interest.

DATA AVAILABILITY STATEMENT

Data sharing is not applicable to this article as no new data were created or analyzed in this study.

ORCID

Adrian Lomeli-Martin https://orcid.org/0000-0003-2215-3449
Nuzhet Ahamed https://orcid.org/0000-0002-2466-6216
Vinay V. Abhyankar https://orcid.org/0000-0002-8462-3920
Blanca H. Lapizco-Encinas https://orcid.org/0000-0001-6283-8210

REFERENCES

1. Wheeler AR, Throndset WR, Whelan RJ, Leach AM, Zare RN, Liao YH, et al. Microfluidic device for single-cell analysis. Anal Chem. 2003;75:3581–6.
2. Zhou J, Ellis AV, Voelcker NH. Recent developments in PDMS surface modification for microfluidic devices. Electrophoresis. 2010;31:2–16.
3. Jen C-PP, Weng C-HH, Huang C-T Te. Three-dimensional focusing of particles using negative dielectrophoretic force in a microfluidic chip with insulating microstructures and dual planar microelectrodes. Electrophoresis. 2011;32:2428–35.
4. Yi GR, Thorsen T, Manoharan VN, Hwang MJ, Jeon SJ, Pine DJ, et al. Generation of uniform colloidal assemblies in soft microfluidic devices. Adv Mater. 2003;15:1300–4.
5. Schultz KM, Furst EM. High-throughput rheology in a microfluidic device. Lab Chip. 2011;11:3802–9.
6. Tegenfeldt JO, Prinz C, Cao H, Huang RL, Austin RH, Chou SY, et al. Micro- and nanofluidics for DNA analysis. Anal Bioanal Chem. 2004;378:1678–92.
7. Abate AR, Thiele J, Weinhart M, Weitz DA. Patterning microfluidic device wettability using flow confinement. Lab Chip. 2010;10:1774–6.
8. Rhee SW, Taylor AM, Tu CH, Cribbs DH, Cotman CW, Jeon NL. Patterned cell culture inside microfluidic devices. Lab Chip. 2005;5:102–7.
9. Ohno KI, Tachikawa K, Manz A. Microfluidics: Applications for analytical purposes in chemistry and biochemistry. Electrophoresis. 2008;29:4443–53.

10. Verpoorte E, De Rooij NF. Microfluidics meets MEMS. Proc IEEE. 2003;91:930–53.
11. Chen X, Cui DF, Liu CC. On-line cell lysis and DNA extraction on a microfluidic biochip fabricated by microelectromechanical system technology. Electrophoresis. 2008;29:1844–51.
12. Nock V, Blaikie RJ, David T. Patterning, integration and characterisation of polymer optical oxygen sensors for microfluidic devices. Lab Chip. 2008;8:1300–7.
13. Chen C, Hirdes D, Folch A. Gray-scale photolithography using microfluidic photomasks. Proc Natl Acad Sci U S A. 2003;100:1499–1504.
14. Hosseini N, Olokede SS, Daneshmand M. A novel miniaturized asymmetric CPW split ring resonator with extended field distribution pattern for sensing applications. Sensors Actuators, A Phys. 2020;304:111769.
15. Stone HA, Kim S. Microfluidics: Basic issues, applications, and challenges. AIChE J 2001;47:1250–4.
16. Kobayashi Y, Sakai M, Ueda A, Maruyama K, Saiki T, Suzuki K. Writing and reading methodology for biochips with sub-100-nm chemical patterns based on near-field scanning optical microscopy. Anal Sci. 2008;24:571–6.
17. Palli G. Miniaturized Optical-based Force Sensors for Tendon-driven Robots. 2011;5344–9.
18. Kollipara PS, Li J, Zheng Y. Optical Patterning of Two-Dimensional Materials. Research. 2020;2020:1–15.
19. Fassbender J, McCord J. Magnetic patterning by means of ion irradiation and implantation. J Magn Magn Mater. 2008;320:579–96.
20. Cheng X, Guo LJ. A combined-nanoimprint-and-photolithography patterning technique. Microelectron Eng. 2004;71:277–82.
21. Gagnon ZR. Cellular dielectrophoresis: Applications to the characterization, manipulation, separation and patterning of cells. Electrophoresis. 2011;32:2466–87.
22. Hahn MS, Taite LJ, Moon JJ, Rowland MC, Ruffino KA, West JL. Photolithographic patterning of polyethylene glycol hydrogels. Biomaterials. 2006;27:2519–24.
23. Yager KG, Barrett CJ. All-optical patterning of azo polymer films. Curr Opin Solid State Mater Sci. 2001;5:487–94.
24. Kato T, Oshima D, Iwata S. Ion irradiation for planar patterning of magnetic materials. Crystals. 2019;9:1–13.
25. Arnold WM. Particle patterning using fluidics and electric fields. IEEE Trans Dielectr Electr Insul. 2008;15:144–51.
26. Liang W, Zhao Y, Liu L, Wang Y, Dong Z, JungLi W et al. Rapid and label-free separation of burkitt's lymphoma cells from red blood cells by optically-induced electrokinetics. PLoS One. 2014;9:1–9.
27. Gao J, Sin MLY, Liu T, Gau V, Liao JC, Wong PK. Hybrid electrokinetic manipulation in high-conductivity media. Lab Chip. 2011;11:1770–5.
28. Gong JR. Label-free attomolar detection of proteins using integrated nanoelectronic and electrokinetic devices. Small. 2010;6:967–73.
29. Khandelwal A, Athreya N, Tu MQ, Janavicius LL, Yang Z, Milenkovic O et al. Self-assembled microtubular electrodes for on-chip low-voltage electrophoretic manipulation of charged particles and macromolecules. Microsystems Nanoeng. 2022 81 2022;8:1–12.
30. Song Y, Yu W, Liu Z, Huang Y, Li M, Li D. Electrokinetic transportation and differentiation of copper and aluminum particles in oil with an oil-water interface. Colloids Surfaces A Physicochem Eng Asp. 2022;641:128397.
31. Zhou T, Michaels M, Kulinsky L. Guided healing of damaged microelectrodes via electrokinetic assembly of conductive carbon nanotube bridges. Micromachines. 2021;12:1–13.
32. Lochab V, Prakash S. Combined electrokinetic and shear flows control colloidal particle distribution across microchannel cross-sections. Soft Matter. 2021;17:611–20.
33. Krishna S, Alnaimat F, Hilal-Alnaqbi A, Khashan S, Mathew B. Dielectrophoretic microfluidic device for separating microparticles based on size with sub-micron resolution. Micromachines. 2020;11:1–17.
34. Abdallah BG, Zatsepin NA, Roy-Chowdhury S, Coe J, Conrad CE, Dörner K, et al. Microfluidic sorting of protein nanocrystals by size for X-ray free-electron laser diffraction. Struct Dyn. 2015;2. https://doi.org/10.1063/1.4928688
35. Hanauer M, Pierrat S, Zins I, Lotz A, Sönnichsen C. Separation of nanoparticles by gel electrophoresis according to size and shape. Nano Lett. 2007;7:2881–5.
36. Chang H, Li D, Zhang X, Xu R, Zhang J, Song Y. Size-dependent electrophoretic motion of polystyrene particles at polyethylene glycol–dextran interfaces. Electrophoresis. 2022;2112–9.
37. Wong PK, Wang TH, Deval JH, Ho CM. Electrokinetics in micro devices for biotechnology applications. IEEE/ASME Trans Mechatronics. 2004;9:366–76.
38. Henderson D, Boda D. Insights from theory and simulation on the electrical double layer. Phys Chem Chem Phys. 2009;11:3822–30.
39. Alizadeh A, Hsu WL, Wang M, Daiguji H. Electroosmotic flow: From microfluidics to nanofluidics. Electrophoresis. 2021;42:834–68.
40. Lacher NA, Garrison KE, Scott Martin R, Lunte SM. Microchip capillary electrophoresis/electrochemistry. Electrophoresis. 2001;22:2526–36.
41. Luo RH, Keh HJ. Electrophoresis and electric conduction in a salt-free suspension of charged particles. Electrophoresis. 2021;42:2134–42.
42. Lapizco-Encinas BH. The latest advances on nonlinear insulator-based electrokinetic microsystems under direct current and low-frequency alternating current fields: a review. Anal Bioanal Chem. 2022;414:885–905.
43. Lian M, Islam N, Wu J. Particle Line Assembly/Patterning by Microfluidic AC Electroosmosis. J Phys Conf Ser. 2006;34:589.
44. Çetin B, Li D. Dielectrophoresis in microfluidics technology. Electrophoresis. 2011;32:2410–27.
45. Pethig R. Dielectrophoresis: Status of the theory, technology, and applications. Biomicrofluidics. 2010; 4. https://doi.org/10.1063/1.3456626
46. Abd Rahman N, Ibrahim F, Yafouz B, Rahman NA, Ibrahim F, Yafouz B. Dielectrophoresis for Biomedical Sciences Applications: A Review. Sensors. 2017;17:449.
47. Rashed MZ, Williams SJ. Advances and applications of isomotive dielectrophoresis for cell analysis. Anal Bioanal Chem. 2020 41216 2020;412:3813–33.
48. Haw MD. Colloidal suspensions, brownian motion, molecular reality: A short history. J Phys Condens Matter. 2002;14:7769–79.
49. Jeong S, Naidu G, Leiknes T, Vigneswaran S. *Membrane biofouling: Biofouling assessment and reduction strategies in sea-*

water reverse osmosis desalination. Elsevier Ltd., 2017; https://doi.org/10.1016/b978-0-12-409547-2.12261-9
50. Sicard F, Striolo A. *Computational simulations for particles at interfaces*. 2018; https://doi.org/10.1016/B978-0-12-804069-0.00006-X
51. Goel M, Singh A, Bhola A, Gupta S. Size-Tunable Assembly of Gold Nanoparticles Using Competitive AC Electrokinetics. Langmuir 2019;35:8015–24.
52. Shipway AN, Katz E, Willner I. Nanoparticle arrays on surfaces for electronic, optical, and sensor applications. Angew Chemie. (International Ed English) 2000;39:19–52.
53. Velev OD, Lenhoff AM, Kaler EW. A Class of Microstructured Particles Through Colloidal Crystallization. Science. (80-) 2000;287:2240–43.
54. Cayre O, Paunov VN, Velev OD. Fabrication of asymmetrically coated colloid particles by microcontact printing techniques. J Mater Chem. 2003;13:2445–50.
55. Velev OD, Kaler EW. Structured porous materials via colloidal crystal templating: from inorganic oxides to metals. Adv Mater. 2000;12:531–4.
56. Dies H, Nosrati R, Raveendran J, Escobedo C, Docoslis A. SERS-from-scratch: An electric field-guided nanoparticle assembly method for cleanroom-free and low-cost preparation of surface-enhanced Raman scattering substrates. Colloids Surfaces A Physicochem Eng Asp. 2018;553:695–702.
57. Fernández-Mateo R, Calero V, Morgan H, García-Sánchez P, Ramos A. Wall Repulsion of Charged Colloidal Particles during Electrophoresis in Microfluidic Channels. Phys Rev Lett. 2022;128. https://doi.org/10.1103/PhysRevLett.128.074501
58. Muto H, Amano T, Wai •, Tan K, Yokoi A, Kawamura Go et al. Ordered arrays of electrostatically assembled SiO2–SiO2 composite particles by electrophoresis-induced stimulation. J Sol-Gel Sci Technol. 2022 2022;1–10.
59. Bi J, Qi X. Oxidation and oriented attachment growth of colloidal nanoparticles during electrophoretic deposition. Mater Lett. 2022;324:132671.
60. Hayward RC, Saville DA, Aksay IA. Electrophoretic assembly of colloidal crystals with optically tunable micropatterns. Nature. 2000;404:56–9.
61. Woehl TJ, Heatley KL, Dutcher CS, Talken NH, Ristenpart WD. Electrolyte-dependent aggregation of colloidal particles near electrodes in oscillatory electric fields. Langmuir. 2014;30:4887–94.
62. Boymelgreen AM, Balli T, Miloh T, Yossifon G. Active colloids as mobile microelectrodes for unified label-free selective cargo transport. Nat Commun. 2018;9:1–8.
63. Shen S, Qin X, Feng H, Xie S, Yi Z, Jin M, et al. Electro-Microfluidic Assembly Platform for Manipulating Colloidal Structures inside Water-in-Oil Emulsion Droplets. Adv Sci. 2022;2203341:1–14.
64. Gong J, Wu N. Electric-Field Assisted Assembly of Colloidal Particles into Ordered Nonclose-Packed Arrays. Langmuir. 2017;33:5769–76.
65. Katzmeier F, Altaner B, List J, Gerland U, Simmel FC. Emergence of Colloidal Patterns in ac Electric Fields. Phys Rev Lett. 2022;128:058002.
66. Li X, Maki KL, Schertzer MJ. Preliminary investigation of the effect of dielectrophoresis on colloidal transport and deposition in eva[1]Li X, Maki KL, Schertzer MJ. Preliminary investigation of the effect of dielectrophoresis on colloidal transport and deposition in evaporating dro. ASME Int Mech Eng Congr Expo Proc. 2018;7:1–7.
67. Mansouri M, Ahmed A, Ahmad SD, McCloskey MC, Joshi IM, Gaborski TR, et al. The Modular μSiM Reconfigured: Integration of Microfluidic Capabilities to Study In Vitro Barrier Tissue Models under Flow. Adv Healthc Mater. 2022. https://doi.org/10.1002/adhm.202200802
68. Gopmandal PP, Duval JFL. Electrostatics and electrophoresis of engineered nanoparticles and particulate environmental contaminants: Beyond zeta potential-based formulation. Curr Opin Colloid Interface Sci. 2022;60:101605.
69. Jayaraman AS, Klaseboer E, Chan DYC. The unusual fluid dynamics of particle electrophoresis. J Colloid Interface Sci. 2019;553:845–63.
70. Ta HY, Collin F, Perquis L, Poinsot V, Ong-Meang V, Couderc F. Twenty years of amino acid determination using capillary electrophoresis: A review. Anal Chim Acta. 2021;1174. https://doi.org/10.1016/j.aca.2021.338233
71. Caires AJ, Castro MM, Montoro LA, Isaac A, Figueiredo RB. Redox reaction in a Mg/Nb2O5 nanocomposite processed by high-pressure torsion. Mater Lett. 2021;303:130418.
72. Al-Ali A, Waheed W, Abu-Nada E, Alazzam A. A review of active and passive hybrid systems based on Dielectrophoresis for the manipulation of microparticles. J Chromatogr A. 2022;1676:463268.
73. Peng C, Wang Y, Sungtaek Ju Y. Finger-powered electrophoretic transport of discrete droplets for portable digital microfluidics. Lab Chip. 2016;16:2521–31.
74. Kim J, Kim T, Ji I, Hong J. Digital Microfluidic Mixing via Reciprocating Motions of Droplets Driven by Contact Charge Electrophoresis. Micromachines. 2022;13. https://doi.org/10.3390/mi13040593
75. Frozanpoor I, Cooke M, Racz Z, Bossons I, Ambukan V, Wood D, et al. Programmable droplet actuating platform using liquid dielectrophoresis. J Micromechanics Microengineering. 2021;31. https://doi.org/10.1088/1361-6439/abf032
76. Brown C V, Edwards AMJ, Roberts A, Newton MI, Sage IC, Ledesma-Aguilar R, et al. Bubble Control, Levitation, and Manipulation Using Dielectrophoresis. Adv Mater Interfaces. 2021;8. https://doi.org/10.1002/admi.202001204
77. Vo Q, Tran T. Mediation of lubricated air films using spatially periodic dielectrophoretic effect. Nat Commun. 2021;12. https://doi.org/10.1038/s41467-021-24534-6
78. Mahapatra P, Ohshima H, Gopmandal PP. Electrophoresis of Dielectric and Hydrophobic Spherical Fluid Droplets Possessing Uniform Surface Charge Density. 2022. https://doi.org/10.1021/acs.langmuir.2c01702
79. Williams MJ, Lee NK, Mylott JA, Mazzola N, Ahmed A, Abhyankar V V. A Low-Cost, Rapidly Integrated Debubbler (RID) Module for Microfluidic Cell Culture Applications. Micromachines. 2019;10:360.
80. Giesler J, Weirauch L, Thöming J, Baune M, Pesch GR. Separating microparticles by material and size using dielectrophoretic chromatography with frequency modulation. Sci Rep. 2021;11:16861.
81. Loo MH, Nakagawa Y, Kim SH, Isozaki A, Goda K. High-throughput sorting of nanoliter droplets enabled by a sequentially addressable dielectrophoretic array. Electrophoresis 2022;43: 477–86.

82. Frozanpoor I, Cooke M, Alvarez-Ruiz D, Ambukan V, Gallant A, Balocco C. Tilting micromirror platform based on liquid dielectrophoresis. Sensors Actuators A Phys. 2021;332:113177.
83. Paiva JS, Jorge PAS, Rosa CC, Cunha JPS. Optical fiber tips for biological applications: From light confinement, biosensing to bioparticles manipulation. Biochim Biophys Acta - Gen Subj. 2018;1862:1209–46.
84. Yasukawa T, Gotoh T, Yasuda T, Suzuki M, Mizutani F. Particle patterning based on positive dielectrophoresis using a scanning microelectrode. Sensors Mater. 2019;31:23–32.
85. Turker E, Arslan-Yildiz A. Recent Advances in Magnetic Levitation: A Biological Approach from Diagnostics to Tissue Engineering. ACS Biomater Sci Eng. 2018;4:787–99.
86. Ino K, Shiku H, Ozawa F, Yasukawa T, Matsue T. Manipulation of microparticles for construction of array patterns by negative dielectrophoresis using multilayered array and grid electrodes. Biotechnol Bioeng. 2009;104:709–18.
87. Albrecht DR, Underhill GH, Wassermann TB, Sah RL, Bhatia SN. Probing the role of multicellular organization in three-dimensional microenvironments. Nat Methods. 2006;3:369–75.
88. Hsiung LC, Yang CH, Chiu CL, Chen CL, Wang Y, Lee H, et al. A planar interdigitated ring electrode array via dielectrophoresis for uniform patterning of cells. Biosens Bioelectron. 2008;24:869–75.
89. Sankara Narayanan TSN, Park IS, Lee MH. Surface Modification of Magnesium and its Alloys for Biomedical Applications. Elsevier Ltd, 2015. https://doi.org/10.1016/C2013-0-16447-1
90. Mora J, Dudoff JK, Moran BD, DeOtte JR, Du Frane WL, Kuntz JD, et al. Projection based light-directed electrophoretic deposition for additive manufacturing. Addit Manuf. 2018;22:330–3.
91. Sopubekova E, Kibar G, Erdem EY. Single, binary and successive patterning of charged nanoparticles by electrophoretic deposition. J Nanoparticle Res. 2021;23:1–12.
92. Kale A, Patel S, Qian S, Hu G, Xuan X. Joule heating effects on reservoir-based dielectrophoresis. Electrophoresis. 2014;35:721–7.
93. Zhang J, Yuan D, Zhao Q, Yan S, Tang SY, Tan SH, et al. Tunable particle separation in a hybrid dielectrophoresis (DEP)- inertial microfluidic device. Sensors Actuators, B Chem. 2018;267:14–25.
94. Li X, Duan J, Qu Z, Wang J, Ji M, Zhang B. Continuous Particle Separation Driven by 3D Ag-PDMS Electrodes with Dielectric Electrophoretic Force Coupled with Inertia Force. Micromachines. 2022;13. https://doi.org/10.3390/MI13010117
95. Romero-Creel MF, Goodrich E, Polniak D V., Lapizco-Encinas BH. Assessment of sub-micron particles by exploiting charge differences with dielectrophoresis. Micromachines. 2017;8. https://doi.org/10.3390/mi8080239
96. Saucedo-Espinosa MA, Rauch MM, LaLonde A, Lapizco-Encinas BH. Polarization behavior of polystyrene particles under direct current and low-frequency (<1 kHz) electric fields in dielectrophoretic systems. Electrophoresis. 2016;37:635–44.
97. Kumar A, Kwon JS, Williams SJ, Green NG, Yip NK, Wereley ST. Optically modulated electrokinetic manipulation and concentration of colloidal particles near an electrode surface. Langmuir. 2010;26:5262–72.
98. Work AH, Williams SJ. Characterization of 2D colloids assembled by optically-induced electrohydrodynamics. Soft Matter. 2015;11:4266–72.
99. Williams SJ, Kumar A, Wereley ST. Optically induced electrokinetic patterning and manipulation of particles. Phys Fluids. 2009;21:91103–4.
100. Williams SJ, Kumar A, Green NG, Wereley ST. Optically induced electrokinetic concentration and sorting of colloids. J Micromechanics Microengineering. 2010;20. https://doi.org/10.1088/0960-1317/20/1/015022
101. Weirauch L, Lorenz M, Hill N, Lapizco-Encinas BH, Baune M, Pesch GR, et al. Material-selective separation of mixed microparticles via insulator-based dielectrophoresis. Biomicrofluidics. 2019;13:064112.
102. Polniak D V, Goodrich E, Hill N, Lapizco-Encinas BH. Separating large microscale particles by exploiting charge differences with dielectrophoresis. J Chromatogr A. 2018;1545:84–92.
103. Kale A, Patel S, Xuan X. Three-dimensional reservoir-based dielectrophoresis (rDEP) for enhanced particle enrichment. Micromachines. 2018;9. https://doi.org/10.3390/mi9030123
104. Shi L, Zhong X, Ding H, Yu Z, Jin J, Zhou T, et al. Continuous separation of microparticles based on optically induced dielectrophoresis. Microfluid Nanofluidics. 2022;26:6.
105. Liu W, Tao Y, Xue R, Song C, Wu Q, Ren Y. Continuous-Flow Nanoparticle Trapping Driven by Hybrid Electrokinetics in Microfluidics. Electrophoresis. 2021;42:939–49.
106. Iliescu C, Xu G, Tong WH, Yu F, Bălan CM, Tresset G, et al. Cell patterning using a dielectrophoretic–hydrodynamic trap. Microfluid Nanofluidics. 2015;19:363–73.
107. Guillotin B, Guillemot F. Cell patterning technologies for organotypic tissue fabrication. 2011.
108. Albrecht DR, Tsang VL, Sah RL, Bhatia SN. Photo- and electropatterning of hydrogel-encapsulated living cell arrays. Lab Chip. 2005;5:111–8.
109. Dai X, Knupp SA, Xu Q. Patterning nanoparticles in a three-dimensional matrix using an electric-field-assisted gel transferring technique. Langmuir. 2012;28:2960–4.
110. Ho CT, Lin RZ, Chang WY, Chang HY, Liu CH. Rapid heterogeneous liver-cell on-chip patterning via the enhanced field-induced dielectrophoresis trap. Lab Chip. 2006;6:724–34.
111. Coll De Peña A, Miller A, Lentz CJ, Hill N, Parthasarathy A, Hudson AO. Creation of an electrokinetic characterization library for the detection and identification of biological cells. Anal Bioanal Chem. 2020;412:3935–45.
112. Brisson V, Tilton RD. Self-assembly and two-dimensional patterning of cell arrays by electrophoretic deposition. Biotechnol Bioeng. 2001;77:290–5.
113. Neirinck B, Van Mellaert L, Fransaer J, Van der Biest O, Anné J, Vleugels J. Electrophoretic deposition of bacterial cells. Electrochem commun. 2009;11:1842–5.
114. Goel M, Verma A, Gupta S. Electric-field driven assembly of live bacterial cell microarrays for rapid phenotypic assessment and cell viability testing. Biosens Bioelectron. 2018;111:159–65.
115. Henslee EA, Dunlop CM, De Mel CM, Carter EA, Abdallat RG, Camelliti P, et al. DEP-Dots for 3D cell culture: low-cost, high-repeatability, effective 3D cell culture in multiple gel systems. 2020;10:14603.
116. Hoettges KF, Hübner Y, Broche LM, Ogin SL, Kass GEN, Hughes MP. Dielectrophoresis-activated multiwell plate for label-free high-throughput drug assessment. Anal Chem. 2008;80:2063–8.

117. Lalonde A, Romero-Creel MF, Lapizco-Encinas BH. Assessment of cell viability after manipulation with insulator-based dielectrophoresis. Electrophoresis. 2015;36:1479–84.
118. Wang XB, Huang Y, Burt JPH, Markx GH, Pethig R. Selective dielectrophoretic confinement of bioparticles in potential energy wells. J Phys D Appl Phys. 1993;26:1278–85.
119. Verduzco-Luque CE, Alp B, Stephens GM, Markx GH. Construction of biofilms with defined internal architecture using dielectrophoresis and flocculation. Biotechnol Bioeng. 2003;83:39–44.
120. Alp B, Stephens GM, Markx GH. Formation of artificial, structured microbial consortia (ASMC) by dielectrophoresis. Enzyme Microb Technol. 2002;31:35–43.
121. Sebastian A, Buckle AM, Markx GH. Formation of multilayer aggregates of mammalian cells by dielectrophoresis. J Micromechanics Microengineering. 2006;16:1769–77.
122. Zhu K, Kaprelyants AS, Salina EG, Schuler M, Markx GH. Construction by dielectrophoresis of microbial aggregates for the study of bacterial cell dormancy. Biomicrofluidics. 2010;4. https://doi.org/10.1063/1.3435336
123. Krause F. Detection and analysis of protein-protein interactions in organellar and prokaryotic proteomes by native gel electrophoresis: (Membrane) protein complexes and supercomplexes. Electrophoresis. 2006;27:2759–81.
124. Peppas NA, Bures P, Leobandung W, Ichikawa H. Hydrogels in pharmaceutical formulations. Eur J Pharm Biopharm. 2000;50:27–46.
125. Lee KY, Mooney DJ. Hydrogels for tissue engineering. Chem Rev. 2001;101:1869–79.
126. Abhyankar V V., Beebe DJ. Spatiotemporal micropatterning of cells on arbitrary substrates. Anal Chem. 2007;79:4066–73.
127. Gillette BM, Rossen NS, Das N, Leong D, Wang M, Dugar A, et al. Engineering extracellular matrix structure in 3D multiphase tissues. Biomaterials. 2011;32:8067–76.
128. Abhyankar V V, Toepke MW, Cortesio CL, Lokuta MA, Huttenlocher A, Beebe DJ. A platform for assessing chemotactic migration within a spatiotemporally defined 3D microenvironment. Lab Chip. 2008;8:1507–15.
129. Abhyankar V V, Wu M, Koh CY, Hatch A V A. Reversibly Sealed, Easy Access, Modular (SEAM) Microfluidic Architecture to Establish In Vitro Tissue Interfaces. PLoS One. 2016;11:e0156341.
130. Dolník V, Liu S, Jovanovich S. Capillary electrophoresis on microchip. Electrophoresis. 2000;21:41–54.
131. Tsai YC, Jen HP, Lin KW, Hsieh YZ. Fabrication of microfluidic devices using dry film photoresist for microchip capillary electrophoresis. J Chromatogr A. 2006;1111:267–71.
132. Ahmed A, Joshi IM, Mansouri M, Ahamed NNN, Hsu MC, Gaborski TR, et al. Engineering fiber anisotropy within natural collagen hydrogels. Am J Physiol - Cell Physiol. 2021;320:C1112–4.
133. Wei J, Han J, Zhao Y, Cui Y, Wang B, Xiao Z, et al. The importance of three-dimensional scaffold structure on stemness maintenance of mouse embryonic stem cells. Biomaterials. 2014;35:7724–33.
134. Ahmed A, Joshi IM, Larson S, Mansouri M, Gholizadeh S, Allahyari Z, et al. Microengineered 3D Collagen Gels with Independently Tunable Fiber Anisotropy and Directionality. Adv Mater Technol. 2021;6:1–10.
135. Ahmed A, Mansouri M, Joshi IM, Byerley AM, Day SW, Gaborski TR, et al. Local extensional flows promote long-range fiber alignment in 3D collagen hydrogels. Biofabrication. 2022;14. https://doi.org/10.1088/1758-5090/ac7824
136. Fechine GJM, Barros JAG, Catalani LH. Poly(N-vinyl-2-pyrrolidone) hydrogel production by ultraviolet radiation: New methodologies to accelerate crosslinking. Polymer (Guildf). 2004;45:4705–9.
137. Turner NW, Jeans CW, Brain KR, Allender CJ, Hlady V, Britt DW. From 3D to 2D: A review of the molecular imprinting of proteins. Biotechnol Prog. 2006;22:1474–89.
138. Hoyle CE, Lowe AB, Bowman CN. Thiol-click chemistry: A multifaceted toolbox for small molecule and polymer synthesis. Chem Soc Rev. 2010;39:1355–87.
139. Abdallat RG, Ahmad Tajuddin AS, Gould DH, Hughes MP, Fatoyinbo HO, Labeed FH. Process development for cell aggregate arrays encapsulated in a synthetic hydrogel using negative dielectrophoresis. Electrophoresis. 2013;34:1059–67.
140. Lee JM, Seo HI, Bae JH, Chung BG. Hydrogel microfluidic co-culture device for photothermal therapy and cancer migration. Electrophoresis. 2017;38:1318–24.
141. Lee Y, Lee JM, Bae PK, Chung IY, Chung BH, Chung BG. Photo-crosslinkable hydrogel-based 3D microfluidic culture device. Electrophoresis. 2015;36:994–1001.
142. Aguilar JP, Lipka M, Primo GA, Licon-Bernal EE, Fernández-Pradas JM, Yaroshchuk A, et al. 3D Electrophoresis-Assisted Lithography (3DEAL): 3D Molecular Printing to Create Functional Patterns and Anisotropic Hydrogels. Adv Funct Mater. 2018;28:1703014.
143. Gargava A, Ahn S, Bentley WE, Raghavan SR. Rapid Electroformation of Biopolymer Gels in Prescribed Shapes and Patterns: A Simpler Alternative to 3-D Printing. ACS Appl Mater Interfaces. 2019;11:37103–11.
144. Isaka K, Kimura Y, Osaka T, Tsuneda S. High-rate denitrification using polyethylene glycol gel carriers entrapping heterotrophic denitrifying bacteria. Water Res 2012;46:4941–8.
145. Schmidt JJ, Rowley J, Hyun JK. Hydrogels used for cell-based drug delivery. J Biomed Mater Res - Part A. 2008;87:1113–22.
146. Afkhami Ardekani M, Ghaffari H. Optimization of prostate brachytherapy techniques with polyethylene glycol–based hydrogel spacers: A systematic review. Brachytherapy. 2020;19:13–23.
147. Karsh LI, Gross ET, Pieczonka CM, Aliotta PJ, Skomra CJ, Ponsky LE, et al. Absorbable Hydrogel Spacer Use in Prostate Radiotherapy: A Comprehensive Review of Phase 3 Clinical Trial Published Data. Urology. 2018;115:39–44.
148. Kim HJ, Choi W, San Lee J, Choi J, Choi N, Hwang KS. Clinical application of serological Alzheimer's disease diagnosis using a highly sensitive biosensor with hydrogel-enhanced dielectrophoretic force. Biosens Bioelectron. 2022;195:113668.

How to cite this article: Lomeli-Martin A, Ahamed N, Abhyankar VV, Lapizco-Encinas BH. Electropatterning—Contemporary developments for selective particle arrangements employing electrokinetics. Electrophoresis. 2023;1–26. https://doi.org/10.1002/elps.202200286